Applied Ocean Research 152 (2024) 104197

Contents lists available at ScienceDirect

Applied Ocean Research

journal homepage: www.elsevier.com/locate/apor

Research paper

On the effects of wind and operating conditions on mooring line tensions for floating offshore wind turbine

A. Lauria [a], P. Loprieno [a,*], F. Rizzo [b], A. Severini [c], D. Foti [b], E. Leone [a], A. Francone [a], G.R. Tomasicchio [a]

[a] Department of Engineering for Innovation, EUMER Campus Ecotekne, University of Salento, Via per Monteroni, Lecce, 73100, Puglia, Italy
[b] Department of Architecture Construction and Design, Polytechnic University of Bari, Via Orabona, Bari, 70125, Puglia, Italy
[c] iLStudio, Engineering & Consulting Studio srl, Via Plinio, Taranto, 74121, Puglia, Italy

ARTICLE INFO

Keywords:
FOWT
Mooring system
Wave-wind interaction
Operating condition
OrcaFlex

ABSTRACT

The present work addresses a significant topic in the current understanding of the structural dynamic behavior of mooring lines for floating offshore wind turbines (FOWT) in operating condition and aims to contribute to the ongoing efforts to enhance the performance and reliability of floating offshore wind energy systems. The present paper investigates the impact of operating conditions on mooring line tension for FOWT. A numerical model of a spar-type FOWT developed in Orcaflex, validated with experimental data, was employed to perform dynamic analyses and to calculate the most probable maximum tension values for scenarios involving wave-only and combined wind-wave actions under various operating conditions. Results indicate that the peak frequency of oscillations is primarily influenced by wave frequency and remain unchanged in operating conditions, but the significant variability in the structure's displacement response leads to a notable fluctuation in tensions within the mooring lines. Specifically, higher tensions are observed in the upwind region while lower tensions are evident in the downwind area. However, for prolonged periods it becomes apparent that operating conditions induce high tension levels across all mooring lines, while also exerting a damping contribution related to wave-induced effects. The study underscores that the primary detrimental factor affecting mooring lines in operating conditions is the widening of the operating tension range.

1. Introduction

As the demand for renewable energy sources continues to grow, floating offshore wind turbines have emerged as a promising technology for harnessing wind energy in deep waters (Breton and Moe, 2009; Esteban et al., 2011; Bilgili et al., 2011). However, several challenges impede the competitiveness of the technology in the market, particularly in the case of floating offshore wind turbines used in deep water applications (Butterfield et al., 2007; Willis et al., 2018; Soares-Ramos et al., 2020). For these reasons, there is a need to strengthen and expand research efforts aimed at mitigating the numerous critical issues associated with this technology.

Investigating the dynamic performance of floating offshore wind turbines stands as a highly contentious and intricate subject within the industry. This area of study encompasses a multitude of facets, ranging from structural dynamics and aerodynamics to hydrodynamics, mooring systems, and control strategies, all interwoven into a single multifaceted challenge (Lauria et al., 2024). The dynamic behavior of floating offshore wind turbines is not uniform and relies on various factors, including the type of floating structure utilized, the mechanical and dynamic characteristics of the structures, and the materials employed. Consequently, the structure's response varies based on the type of structure under consideration and the load conditions it encounters. The interaction between wind and waves is particularly crucial for floating wind turbines, as it significantly impacts their structural responses and dynamic behavior. Grasping the intricate relationship between wind and wave conditions is pivotal for accurately evaluating the performance, stability, and safety of these systems. It is evident that diverse wave and wind load scenarios, along with differences in parked and operational conditions, yield varying responses in terms of displacements, tensions, deformations, and damping.

For example in Goupee et al. (2014) and Koo et al. (2014) the dynamic responses of three floating systems (Spar-Buoy, TLP, Semi-submersible) were compared under wave and wind load conditions using 1 : 50 scale models. The research revealed that the presence of wind did not alter the relative behavior between the systems, suggesting that the predominant effects stem from wave motion. However,

* Corresponding author.
E-mail address: pierpaolo.loprieno@unisalento.it (P. Loprieno).

https://doi.org/10.1016/j.apor.2024.104197
Received 7 June 2024; Received in revised form 1 August 2024; Accepted 20 August 2024

Nomenclature

$FOWT$	Floating offshore wind turbine	TLP	Tension leg platforms
p	Position vector	E	Young's modulus of the mooring line
v	Velocity vector	ν	Poisson's coefficient of the mooring line
$\dot{v}$	Acceleration vector	A_m	Area of the section of mooring line
t	Simulation time	ϵ	Total mean axial strain of the mooring line
$M(p,\dot{v})$	System inertia load	l	Instantaneous length of segment of the mooring line
$C(p,v)$	System damping load	λ	Expansion factor of segment of the mooring line
$K(p)$	System stiffness load	l_0	Unstretched length of segment of the mooring line
$F(p,v,t)$	External load	k_{tt}	Torque coupling of the mooring line
C_a	Added mass and coefficient	τ	Segment twist angle of the mooring line
C_m	Inertia coefficient	c	Damping coefficient of the mooring line
f_w	Weight force of spar buoy	$\frac{dl}{dt}$	Rate of increase of length of the mooring line
m	Mass of spar buoy	f_L	Lift force
g	Gravity acceleration	f_D	Drag force
u_z	Unit vertical vector directed upward	m_z	Pitching moment
f_b	Buoyancy force of spar buoy	w	Dynamic inflow for aerodynamic load
ρ_w	Density of water	c_b	Chord
V_{wet}	Volume of the spar buoy immersed in water	A_s	Product between chord and segment length
f	Hydrodynamic loads	$C_l(\alpha)$	Lift coefficient
Δ	Mass of water displaced by the spar buoy	$C_d(\alpha)$	Drag coefficient
a_f	Acceleration of the fluid	$C_m(\alpha)$	Moment coefficient
a_b	Acceleration of the body relative to the earth	α	Angle of attack
A_d	Drag area of the spar buoy	T_{storm}	Storm duration
v_r	Velocity of the fluid relative to the spar-buoy	MPM	Most probable maximum value
T_e	Axial tensile stress of mooring line	n	Number of peaks
p_i	Inner pressure of the mooring line	μ	Mean period
p_o	Outer pressures of the mooring line	σ	Standard deviation
a_i	Area of the inner sections of mooring line	T_z	Mean up-crossing period
a_o	Area of the outer sections of mooring line	α	Risk parameter
T_w	Wall tension of the mooring line	H, T	Wave height and period
v	Disturbed relative velocity	v_q	Quasi-steady velocity induced by the rotor
v_d	Dynamic induced velocity	a, a'	Axial and tangential induction factors
φ	Local inflow angle	$R(\varphi)$	Residual function
x_r, y_r	Coordinates of the nominal rotor plane	k, k'	Non-dimensional parameters
F	Prandtl tip and hub loss	n_B	Is the blade count
c_{loc}	Is the local chord	r	Projection of the mid-segment frame displacement
γ_i	Empirical coefficients	TSR	Tip Speed Ratio

the overall response was observed to be heightened in the presence of wind. Nevertheless, in Oguz et al. (2018) a TLP typology at a $1:67$ scale model was subjected to regular, irregular waves, and wind action revealing that, in contrast to previous research, wind action significantly contributes to the overall dynamics of the system. Several studies focused on the characterization of the dynamic behavior of floating offshore wind turbines under combined wind-wave actions of diverse natures, while also considering operational circumstances. The influence of these conditions on floating wind turbines presents a composite and intricate subject, encapsulating the impact of various environmental factors like wind, waves, and platform dynamics on energy production and structural response. It is widely recognized that operational conditions markedly affect both the energy production and structural loads of floating wind turbines. Factors such as average wind speed, wind direction, wave characteristics, and floater dynamics all play crucial roles in shaping power output and structural behavior in floating wind turbine systems. In Tomasicchio et al. (2018) a spar-type floating offshore wind turbine is studied experimentally under different wave-wind conditions revealing a distinct influence of waves compared to wind on the structural dynamics. The authors noticed that the rotor dynamics and the gyroscopic effects affect the longitudinal response. In Bahramiasl et al. (2018) a TLP-type floating offshore wind turbine (FOWT) was utilized for experimental testing to evaluate the gyroscopic effect induced by rotor rotation. These theme was also documented in Duan et al. (2016) through tank tests on a $1:50$ scale model of the OC3 Hywind prototype and was found an influence on surge, heave and pitch behavior. This study specifically involved the fluid-induced simulation of rotor rotation, enabling a more precise capture of the

adverse effects stemming from rotational speed control. In Feist et al. (2021) an experimental quasi-coupled wind-wave test was conducted, illustrating that wind, in conjunction with blade rotation, can induce alterations in the system's response, particularly when occurring at frequencies near the natural frequencies of the system. In Wen et al. (2022) they experimentally note that increasing aerodynamic loads affect the natural frequencies and damping of FOWTs.

From literature is it clear that the impact of wind on floating offshore wind turbines is a critical consideration in the development and operation of these renewable energy systems and the interaction between wind and waves in the marine environment can have significant implications for offshore wind energy production. The interaction between wind and waves in the marine environment has a significant impact on the fatigue life of offshore wind turbines and then have a considerable impact on long-term effect (Aggarwal et al., 2017; Riefolo et al., 2018; Lee et al., 2023). Research has shown that the combined effect of wind and wave loading can lead to increased fatigue damage and reduced fatigue life of critical components in offshore wind turbines (Saenz-Aguirre et al., 2022; Gao et al., 2021; Barrera et al., 2020; Yang et al., 2020; Li and Zhang, 2020). Mooring systems can be susceptible to failure due to mooring line snap tension (Hsu et al., 2017), which can lead to a substantial increase in tension. These abrupt changes can lead to sudden snap events and reduced safety factors. The coupling effect of mooring line snap tension and anchor out-of-plane loading can significantly impact mooring line tension under extreme conditions, leading to increased tension and potential failure (Xu et al., 2023). Therefore, understanding and accurately assessing the impact of wave-wind interactions on the fatigue life of offshore wind turbines is essential for ensuring their long-term structural reliability and safety. The mooring system is a critical component of floating offshore structures (Chakrabarti, 1994, 2005), playing a pivotal role in maintaining their position and stability during engineering operations and these conditions influence the selection of mooring components, the station-keeping performance requirements, and the long-term inspection, maintenance, and repair requirements (Bae et al., 2017; Zhang et al., 2022). The dynamics of the mooring system is mainly induced by the platform motions through the fairleads, which are influenced by both wind and wave conditions, leading to increased design tensions and potential impact on the overall behavior of the floating wind turbine. While the influence of wind-wave interactions and operational conditions on the dynamic response of floating offshore wind turbines has been extensively studied and debated, there has been limited focus on how these factors directly affect the mooring system and the induced tensions. For these reason the dynamic response of the mooring system to combined wave-wind action and operating conditions, and particularly the stresses to which they are subjected during these conditions presents significant challenges that must be addressed to ensure the reliability and efficiency of these structures.

The primary objective of this study is to isolate and analyze the impact of wind and turbine operational conditions on mooring line tensions, identifying the variations of this impact over both short-term and long-term periods. This paper aims to address this research topic and fill this gap by conducting a comprehensive analysis of mooring line tensions, providing valuable insights into the effects of operating conditions on the mooring systems of floating offshore wind turbines, focusing on the typical three mooring line configuration of a spar type FOWT. The first section presents experimental tests with regular wave action, which were used to validate the numerical model presented in the subsequent section. The effects on mooring lines tension induced by combined wave-wind load actions and operating condition was numerically analyzed with OrcaFlex using dynamic regime analysis and statistically analyzed using the most probable maximum value theory. The results and discussion are reported in the third section and finally there are conclusions.

Table 1
Downscaled properties of spar-buoy OC3-Hywind Froude scale 1 : 40.

Spar-buoy properties	Units	Scale factor	Model scale
Diameter upper cylinder	m	λ	0.163
Diameter lower cylinder	m	λ	0.235
Total draft	m	λ	3
Depth to top of taper below SWL	m	λ	0.1
Depth to bottom of taper below SWL	m	λ	0.3
Center of gravity below SWL	m	λ	2.25
Mass including ballast	kg	λ^3	116.66
Roll inertia	kg m^2	λ^3	41.3
Pitch inertia	kg m^2	λ^3	41.3
Yaw inertia	kg m^2	λ^3	1.6
Elevation to platform top (tower base) above SWL	m	λ	0.3

2. Material and methods

2.1. Experimental model

The dataset used in the present work is derived from the experimental tests (Fig. 1) conducted at the DHI Offshore Wave Basin in Hørsholm, Denmark, within the Hydralab EU funded research project (Tomasicchio et al., 2020; Russo et al., 2021). The DHI wave basin dimensions are 20 m in length, 30 m in width, and has a depth of 3 meters. At the basin's center, a 3 m by 3 m pit with a depth of 6 m is installed. The strategic placement of the tested floating structure within this central pit allowed for the establishment of deep-water conditions. The wave generator comprises 60 individually controlled flaps with a paddle length of 1.5 m, capable of generating regular and irregular waves, directional and unidirectional waves. On the opposite side, there is a 6.5 m wave absorber designed to minimize reflection effects. Nine wave gauges, three positioned in front of the structure and six behind it, have been used to capture the free surface elevation, arranged perpendicular to the wave direction. To monitor the six-degrees-of-freedom motion of the FOWT, a non-contact optical tracking system and three accelerometers are employed. Additionally, a strain gauge load cell with a maximum load capacity of 300 N has been installed to measure tension force on the mooring line.

The floating structure used in the Hydralab+ experimental campaign is a Froude 1 : 40 scale model of the prototype developed in Phase IV of the OC3-Hywind project. Further details can be found in Table 1. The Hydralab+ wind turbine is a 1:40 scale model of the NREL 5MW reference turbine, designed according to Froude similarity rules to match the reference thrust and torque. The rotor is a geometric upscale of the PoliMi WTM, a 1:75 model of the DTU 10MW RWT (Bak et al., 2013; Bayati et al., 2016, 2017), using the SD7032 airfoil for improved performance at lower Reynolds numbers. Near the blade root, the section shape transitions smoothly to a circular section. The model is equipped with four actuators: a main shaft motor for controlling rotor angular speed and three dedicated motors for real-time individual blade pitch adjustments. It also includes an encoder sensor that measures generator speed, providing feedback for the control system. An embedded system manages the actuators and acquires sensor data simultaneously. The control strategy is based on a variable-speed, variable-pitch approach and operates in three distinct regions. In region 1, wind speeds is up to the cut-in speed, facilitating turbine start-up. In region 2, between cut-in and rated wind speeds, the turbine operates at partial load with fixed minimum blade pitch and variable rotor speed to optimize power extraction via torque control. In region 3, from rated to cut-off wind speeds, the generator torque is set to the rated value and turbine operation is regulated by a blade pitch-to-feather PI

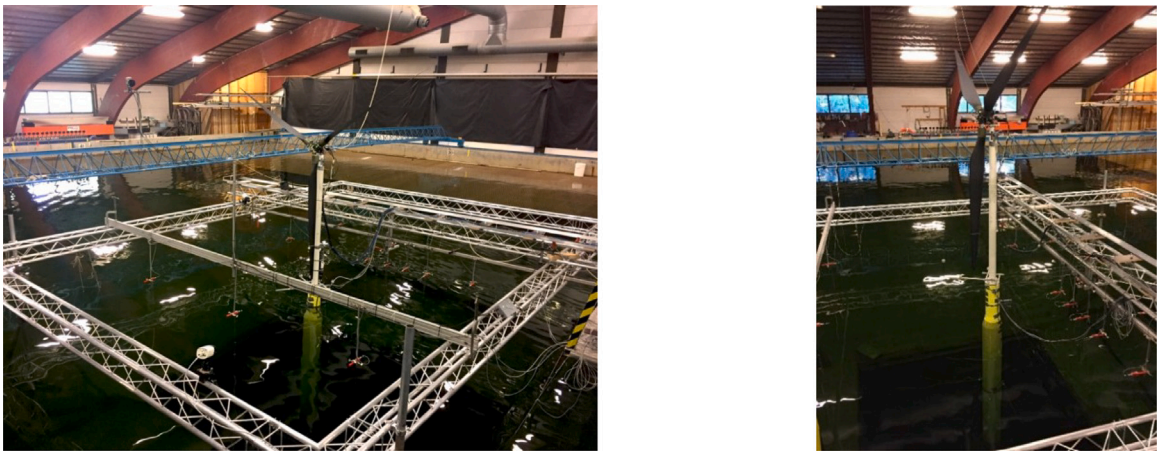

(a) (b)

Fig. 1. Photos of the Hydralab+ experimental campaign conducted at the DHI Offshore Wave Basin in Hørsholm, Denmark.

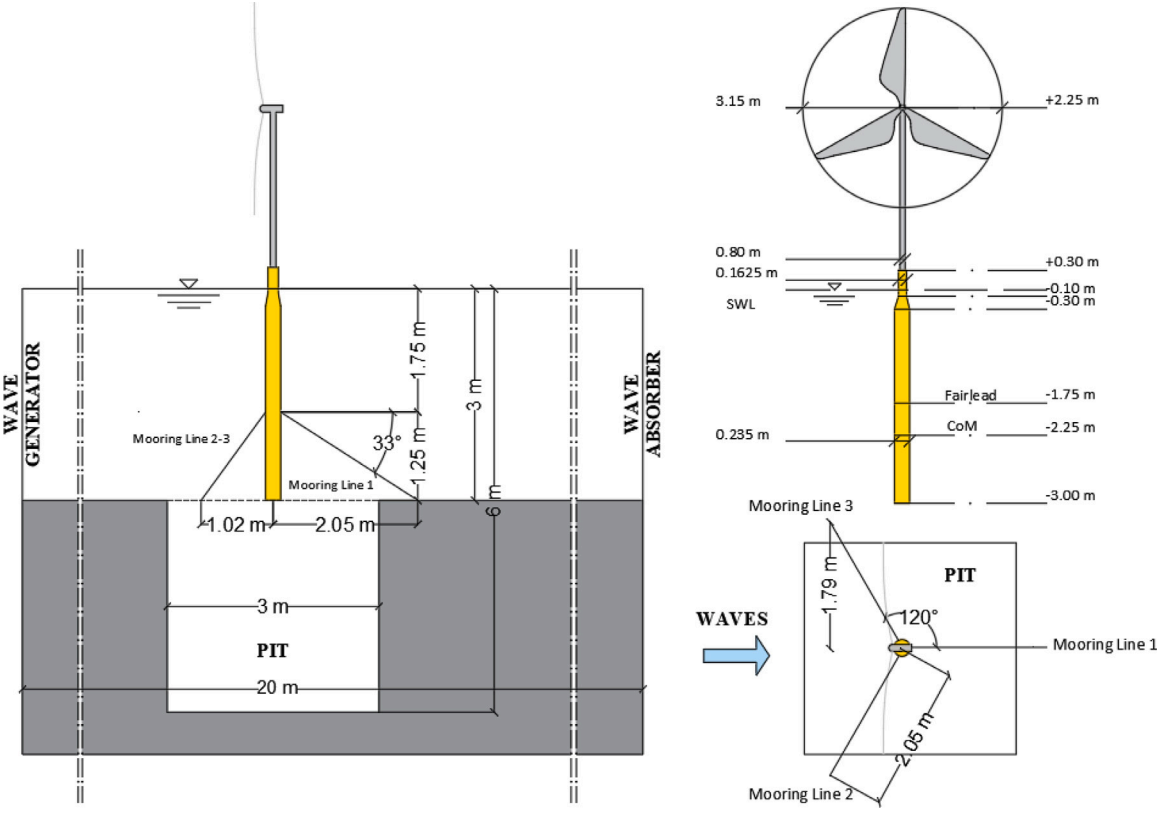

Fig. 2. 1 : 40 FOWT Spar-type model and mooring system configuration adopted during the experimental campaign.

controller. Details regarding the downscaled model and scale factor are summarized in Table 2. Due to the limited depth of the tank and then the impossibility of defining the entire mooring system, the truncation method was adopted. The literature suggests that truncating mooring lines is a viable solution for approximating the behavior of full-scale mooring lines, thereby avoiding the need for excessively small-scale physical models (Chen et al., 2000; Tomasicchio et al., 2017; Stansberg et al., 2002; Fan et al., 2017). To minimize uncertainty, special attention was given to defining the truncated configuration of the mooring lines in order to replicate the equivalent static characteristics of the full-scale system (Stansberg et al., 2004; ITTC, 2021a,b). The mooring system comprises three mooring lines composed of a series of seven springs, with two positioned in front of the model and one behind, forming 120° angles to each other in the horizontal plane. These mooring lines are connected to the spar through a collar positioned 1.75 m below the water level. The anchoring system is truncated at a depth of 3 m and at a horizontal distance of 2.05 m, pre-tensioned using three concrete blocks. Details regarding the location and characteristics of the mooring lines are provided in Table 3. A graphical representation of the described structure is presented in Fig. 2.

2.2. Numerical model

The numerical model represented in Fig. 3 was built using OrcaFlex which is the preeminent software suite for the dynamic analysis of offshore maritime systems, notable for its extensive range of technical

Table 2
Downscaled properties of wind turbine Froude scale 1 : 40.

Wind turbine properties	Units	Scale factor	Model scale
Ideal power	W	$\sqrt{\lambda^7}$	12.35
Gearbox ratio	–	–	42
Rotor orientation	–	–	Clockwise, Upwind
Configuration	–	–	3 Blades
Airfoils	–	–	SD7032s
Control	–	–	Variable Speed, Collective Pitch
Drivetrain	–	–	High Speed, Multiple-Stage Gearbox
Rotor diameter	m	λ	3.15
Hub diameter	m	λ	0.0075
Tower diameter	m	λ	0.08
Elevation to tower base above SWL	m	λ	0.25
Elevation to tower top above SWL	m	λ	2.19
Hub height	m	λ	2.25
Cut-in wind speed	m/s	$\sqrt{\lambda}$	0.5
Rated wind speed	m/s	$\sqrt{\lambda}$	1.8
Cut-out wind speed	m/s	$\sqrt{\lambda}$	4
Cut-in rotor speed	rpm	λ	43.7
Rated rotor speed	rpm	λ	76.5
Rotor mass	kg	λ^3	1.72
Nacelle mass	kg	λ^3	3.75
Single blade mass	kg	λ^3	0.21

Table 3
Downscaled properties of mooring system Froude scale 1 : 40.

Mooring-line properties	Units	Scale factor	Model scale
Number of mooring lines	–	–	3
Horizontal angle between adjacent lines	°	–	120
Vertical angle between floater and lines	°	–	32.6
Depth to anchors below SWL	m	λ	3
Depth to fairleads below SWL	m	λ	1.75
Radius to anchors from platform centerline	m	λ	2.05
Spring pretension	kg	λ^3	1.5
Unstretched spring length	m	λ	1.21
Stretched spring length	m	λ	1.75
Equivalent springs extensional stiffness	N/m	λ^2	27.25

capabilities (summarized in Table 4 Lauria et al., 2024) and its intuitive user interface.

A dynamic analysis in time domain was conducted. Note that p, v, $\dot{v}$ are the position, velocity and acceleration vectors respectively and t the simulation time, the equation of motion solved by OrcaFlex have the following formulation:

$$M(p,\dot{v}) + C(p,v) + K(p) = F(p,v,t) \tag{1}$$

where $M(p,\dot{v})$ is the system inertia load, $C(p,v)$ is the system damping load, $K(p)$ is the system stiffness load and $F(p,v,t)$ is the external load. The implicit integration scheme, specifically the generalized-α integration scheme (Chung and Hulbert, 1993), was utilized for simulation purposes. This scheme offers controllable numerical damping, which is beneficial for eliminating non-physical high-frequency responses and ensures stable convergence, thereby resulting in faster simulations. For each free body and node of the model, acting forces and moments are calculated to solve the equation of motion instantaneously. The floating structure was modeled as a rigid body with all six degrees

Table 4
Computational methods included in OrcaFlex software.

OrcaFlex			
Category	Acronyms	Computational methods	Fidelity levels
Hydrodynamics	PF	Potential Flow	Medium
	QD	Quadratic Drag	Medium
	ME	Morison Equation	Medium
	NA	Newman's Approximation	Medium
	QTF	Quadratic Transfer Function	Medium
Aerodynamics	BEM	Blade Element Momentum	Medium
	GDW	Generalized Dynamic Wake	Medium
	FDT	Filtered Dynamic Thrust	Medium
	DS	Dynamic Stall	Medium
Structural dynamics	R	Rigid	Low
	MOD	Modal	Medium
	MB	Multibody	Medium
	FE	Finite Element	High
Mooring system dynamics	QS	Quasi-Static	Low
	DYN	Dynamic	Medium
	LM	Lumped Mass	Medium
	FE	Finite Element	High

of freedom using the "6Dbuoy-Spar buoy" element, where the overall mass and inertia characteristics are associated with the center of mass. The rigid-body assumption for the spar is considered valid since its deformations are negligible for the overall response. The element's geometry is defined as a sum of co-axial cylindrical finite elements characterized by drag area, added mass C_a, and inertia coefficients C_m. The weight force is computed as:

$$f_w = -mgu_z \tag{2}$$

where m is the mass g is the gravity acceleration and u_z is a unit vertical vector directed upward; for each cylinder into which the geometry is decomposed, the buoyancy force applied at the geometric center is calculated as:

$$f_b = \rho_w g V_{wet} u_z \tag{3}$$

where ρ_w is the density of water and V_{wet} is the volume of the cylinder immersed in water. The hydrodynamic loads are calculated instead through Morison's Equation as follow:

$$f = (C_m \Delta a_f - C_a \Delta a_b) + \frac{1}{2}\rho C_d A_d |v_r| v_r \tag{4}$$

where Δ denotes the mass of water displaced by the body, a_f is the acceleration of the fluid, a_b is the acceleration of the body relative to the earth, A_d is the drag area, and v_r is the velocity of the fluid relative to the body.

In contrast, mooring lines are represented using the "line" element, facilitating concentrated mass modeling. These lines are subsequently divided into a sequence of massless segments, each associated with stiffness characteristics, while the mass properties are concentrated at the nodes. The tension (or axial tensile stress) in the mooring lines is calculated as follows:

$$T_e = T_w + (p_o a_o - p_i a_i) \tag{5}$$

where p_i and p_o are the inner and outer pressures respectively, a_i and a_o represent the area of the inner and outer sections. T_w is the wall tension which depends on axial stiffness, the external and internal pressure through the effect of Poisson's ratio, the torque coupling and the axial damping through a linear or nonlinear definition, as follow:

$$T_w = EA_m\epsilon - 2\nu(p_0 a_0 - p_i a_i) + \kappa_{tt}\frac{\tau}{l_0} + EA_m c\frac{dl}{dt}\frac{1}{t_0} \tag{6}$$

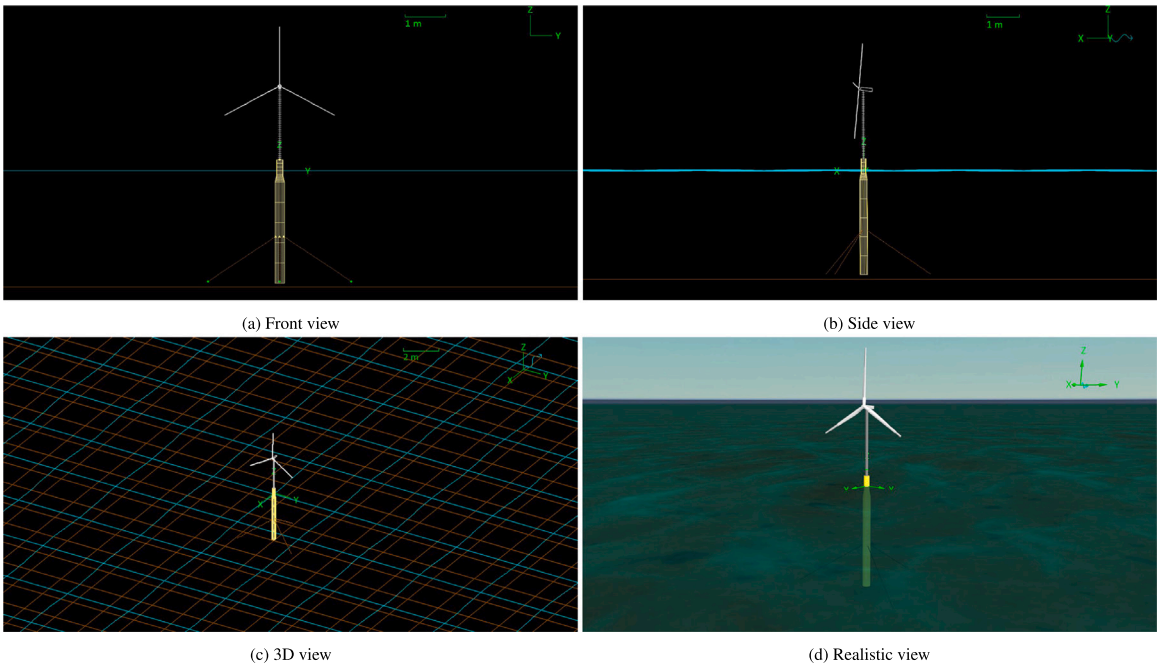

(a) Front view (b) Side view

(c) 3D view (d) Realistic view

Fig. 3. Numerical model of the spar-type floating offshore wind turbine in 1 : 40.

where E is Young's modulus, ν is Poisson's coefficient, A_m the area of the section, $\epsilon = \frac{(l-\lambda l_0)}{(\lambda l_0)}$ is the total mean axial strain with l the instantaneous length of segment, λ expansion factor of segment, l_0 unstretched length of segment, k_{tt} is the torque coupling, τ is the segment twist angle (in radians), c is the damping coefficient, in seconds, and $\frac{dl}{dt}$ is the rate of increase of length. These characteristics of the mooring lines are assigned through the line type "General". The axial, bending, and torsional stiffnesses are input directly and similarly mass is specified per unit length, bypassing the need for calculation based on material density. This direct methodology affords comprehensive control over the data, enabling the analysis of a wide range of flexible structures, including mooring line.

Given the significantly lower stiffness compared to the spar-buoy, the presence of mass at the top due to the rotor-nacelle system, and a fixed constraint at the base capable of absorbing bending moment stresses, tower deformations could impact the overall response under high wind loads. To address this, the tower's deformation capabilities were considered by modeling it using the "line-Homogeneous" element, which calculates comprehensive properties of the overall line type, including geometry, mass, stiffness, and so on. To ensure proper behavior of the line element, it is crucial to define infinite flexural stiffness characteristics at the nodes. Additionally, it is important to evaluate the number of elements used to discretize the spar, tower, and mooring lines through parametric and sensitivity analyses to accurately compute the response.

The nacelle was modeled using the "6dbuoy-Lumped buoy" element, which assigns mass and inertia characteristics to a single point. This element has a more versatile behavior than the spar buoy type, enabling the modeling of any element with six degrees of freedom and any geometry. The rotor was modeled with the "turbine" element, which, starting from the definition and distribution of airfoils on the blades, allows for the complete configuration of the blades in terms of geometry, inertia, and structural characteristics. Additionally, the contributions of mass and inertia from the hub and the generator control system were defined. The blades were modeled as linear elements, discretized into a series of segments, each associated with a predefined airfoil. Each segment was then assigned values for thickness, axial and torsional stiffness, aerodynamic center, neutral axis, chord, twist, and pitch. Aerodynamic loads, including lift force, drag force, and pitching moment, were also incorporated. The aerodynamic loads are calculated individually at the aerodynamic center of each blade's mid-segment frame (Fig. 4). They are due to the inflow w at the specific angle of attack α, which can be in the range between $-180° < \alpha < 180°$, and is expressed by the following relationship:

$$\alpha = \varphi - \text{Effective twist} \tag{7}$$

where φ is the local inflow angle between w and the nominal rotor plane y-axis. Noted that the z-direction, with reference to Fig. 4, points out of the page towards the reader, the lift force, acting in the direction **wxz** follows the equation:

$$f_L = \frac{1}{2}\rho_a A_s C_l(\alpha)|w|^2 \tag{8}$$

The drag force, acting along the **w** direction, is defined as:

$$f_D = \frac{1}{2}\rho_a A_s C_d(\alpha)|w|^2 \tag{9}$$

while the pitching moment, about the z axis, is calculated as:

$$m_z = \frac{1}{2}\rho_a A_s c_b C_m(\alpha)|w|^2 \tag{10}$$

where ρ_a is the density of air, c_b is the chord, A_s is the area of the element obtained as a product between chord and segment length, $C_l(\alpha)$, $C_d(\alpha)$, $C_m(\alpha)$ are respectively the lift, drag and moment coefficients, obtained from the angle of attack α by linear interpolation of the wing profile data. To account for the rotor's induction effects, it is utilized blade element momentum (BEM) theory, which integrates the principles of momentum conservation with classical blade sectional theory. This methodology enables the calculation of axial and tangential induction factors, a and a'. These factors establish the relationship between the quasi-steady velocity induced by the rotor, v_q, and the instantaneous disturbed relative velocity, v, as follows:

$$v = \begin{cases} v_{q,x} = -a v_x \\ v_{q,y} = +a' v_y \\ v_{q,z} = 0 \end{cases} \tag{11}$$

The Øye (1986, 1990) model is used to approximate the dynamic induced velocity, v_d, based on the quasi-steady values. A series of first-order filters are used to transform the quasi-steady induced velocities

into approximations of the dynamic values v_d (Orcina Ltd, 2024). This approach accounts for dynamic effects, offering a more accurate representation of the actual induced velocities during transient conditions. The inflow is then calculated as:

$$w = v + v_d \tag{12}$$

The induction factors are determined by simplifying the problem to one dimension using the local inflow angle φ, as proposed by Ning et al. (2015), solving iteratively for φ the residual function $R(\varphi)$:

$$R(\varphi) = \frac{\sin\varphi}{1-a} - \frac{v_x}{v_y}(1-k\prime)\cos\varphi \tag{13}$$

using a bracketed root finding algorithm. Expressing, for the clockwise rotor case, the lift and drag coefficients relative to the x_r and y_r directions of the nominal rotor plane:

$$C_x(\alpha) = C_l(\alpha)\cos\varphi + C_d(\alpha)\sin\varphi \tag{14}$$

$$C_y(\alpha) = C_d(\alpha)\cos\varphi - C_l(\alpha)\sin\varphi \tag{15}$$

the two non-dimensional parameters can be defined:

$$k = \frac{\sigma C_x(\alpha)}{4F\sin^2\varphi} \tag{16}$$

$$k\prime = \frac{\sigma C_y(\alpha)}{4F\sin\varphi\cos\varphi} \tag{17}$$

where F accounts for Prandtl tip and hub loss, calculated as reported in Orcina Ltd (2024), $\sigma = \frac{n_B c_{loc}}{2\pi r}$, n_B is the blade count, c_{loc} is the local chord, r represents the projection of the mid-segment frame displacement from the turbine origin onto the turbine xy-plan. In operating condition the induction factors are calculated as:

$$a = \begin{cases} \frac{k}{1+k} & \text{if k} \le \frac{2}{3} \\ \frac{\gamma_1 - \sqrt{\gamma_2}}{\gamma_3} & \text{otherwise} \end{cases} \tag{18}$$

$$a\prime = \begin{cases} \frac{k\prime}{1-k\prime} & \text{if } v_x > 0 \\ \frac{-k\prime}{1+k\prime} & \text{otherwise} \end{cases} \tag{19}$$

where γ_i are calculated according to Buhl (2005). The Pitt and Peters skewed wake correction (Pitt and Peters, 1980) is applied retrospectively to the converged axial induction factor a. If the tip speed ratio (TSR) is too low, the BEM theory may become invalid. To address this the induction factors can be optionally scaled with an induction weight, function of TSR (Orcina Ltd, 2024).

2.2.1. Most probable maximum value statistical theory

The methodology for calculating most probable maximum (MPM) value statistics for mooring tensions in OrcaFlex is contingent upon the chosen distribution. In this case, the Rayleigh distribution method is chosen, a direct calculation is employed, relying on the spectral moments of all the available data. The detailed explanation of deriving and utilizing spectral moments for fitting the Rayleigh distribution is provided by Ochi (1998). Under the Gaussian assumption, Ochi demonstrates that the most probable maximum value during a storm duration T_{storm} can be expressed as:

$$MPM = \mu + \sigma(2\ln n)^{\frac{1}{2}} \tag{20}$$

Here, $n = T_{storm}/Tz$ represents the number of peaks, and μ, σ, and T_z denote the mean, standard deviation, and mean up-crossing period, respectively, of the analyzed time series. OrcaFlex provides a report on this most probable extreme value corresponding to the specified storm duration. Ochi proceeds to demonstrate that, at low values of the risk parameter α, the extreme value that will be surpassed with a probability of α is:

$$\mu + \sigma\left\{2ln\left(\frac{n}{\alpha}\right)\right\}^{\frac{1}{2}} \tag{21}$$

However, this approximation is valid only for low values of α. Therefore, OrcaFlex opts for an alternative formula to accurately calculate the extreme value that will be exceeded with a probability of α. Ochi (1973) formulates a more precise expression using Cramér's approximation method in his paper on predicting extreme values. This formula yields reliable results across the entire spectrum of risk factor values (α):

$$\mu + \sigma\left[2ln\left\{\frac{-n}{ln(1-\alpha)}\right\}\right]^{\frac{1}{2}} \tag{22}$$

The Rayleigh distribution method offers several advantages. It allows for the estimation of extreme values, which is crucial for predicting the likelihood of a load exceeding a critical value that may lead to failure. The maximum likelihood fitting procedure used for the Rayleigh distribution enables the estimation of a confidence interval for a specified confidence level, providing valuable information about the uncertainty inherent in the estimated extreme values. Computing extreme values using a risk factor associated with a specific return period allows the maximum expected tension value to be evaluated switching from analyzing a short-term effect to evaluating the long-term effect. Moreover, the use of the Rayleigh distribution method in OrcaFlex aligns with industry standards for offshore wind turbines (Veritas, 2010; DNV, 2011; Det Norske Veritas, 2010; Design, 2005; RP et al., 2014), ensuring that the analysis is conducted in accordance with established best practices.

3. Results and discussion

The experimental tests considered in this study for the validation phase of the numerical model focused solely on reproducing wave action. In contrast, the analysis of aerodynamic loads, turbine operational conditions, and their interactions with wave motion and the resulting effects on mooring line tensions were conducted numerically. The different load combinations considered in this paper are summarized in Table 5. The initial phase focused on validating the numerical model in OrcaFlex by selecting two tests from the experimental campaign (Test 1 and Test 2). These tests refers to two regular wave conditions acting perpendicular to the structure. The wave characteristics are defined by wave heights, H, of 0.05 m and 0.13 m, respectively, and a same wave periods, T, of 1.6 s. Regular waves provide consistent and predictable conditions. This consistency allows for accurate validation of the model under controlled wave conditions. In particular it was chosen to focus on the cases of unidirectional action and perpendicular to the structure because this ensures the maximization of displacements along the degree of freedom of the surge and, as a result, achieves the maximum values of axial tension in the mooring lines. To improve readability and understanding of the results, note that the direction of wave and wind propagation is directed according to the negative direction of the x-axis within the numerical model reference system illustrated in Fig. 3. This validation is essential for ensuring the reliability of the numerical model in predicting the system's response to environmental stress conditions. Below, we present comparisons between the numerical and experimental results in time domain (Figs. 5–6) and using Power Spectral Density (PSD) representation (Figs. 7–8). The numerical model closely aligns with the experimental results, capturing the temporal value trends and frequency peak detection. The calculated percentage errors for the various parameters range from 0.19% to 0.22%, with the exception of the free surface, which exhibits a percentage error of 2.5%.

3.1. Numerical analysis in operating condition

After calibrating the numerical model using the experimental data (Tests 1 and 2), the model was then used to simulate numerically the conditions of Tests 3, 4, 5, and 6. These tests refers to a combination of wave conditions of Tests 1 and 2 with two different wind

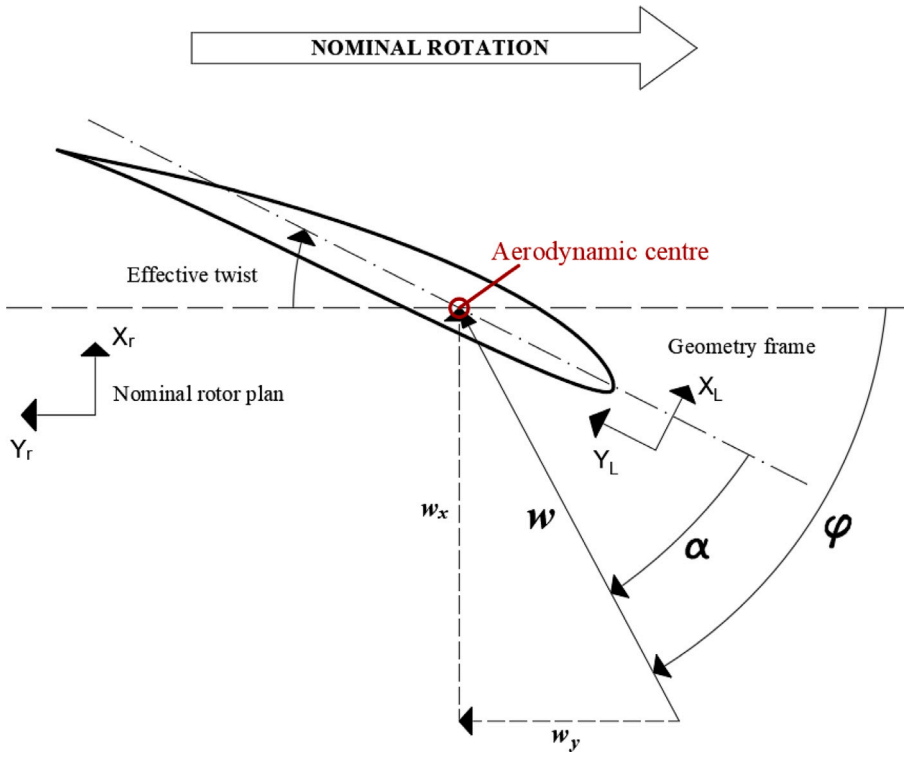

Fig. 4. Direction of inflow for clockwise rotation.

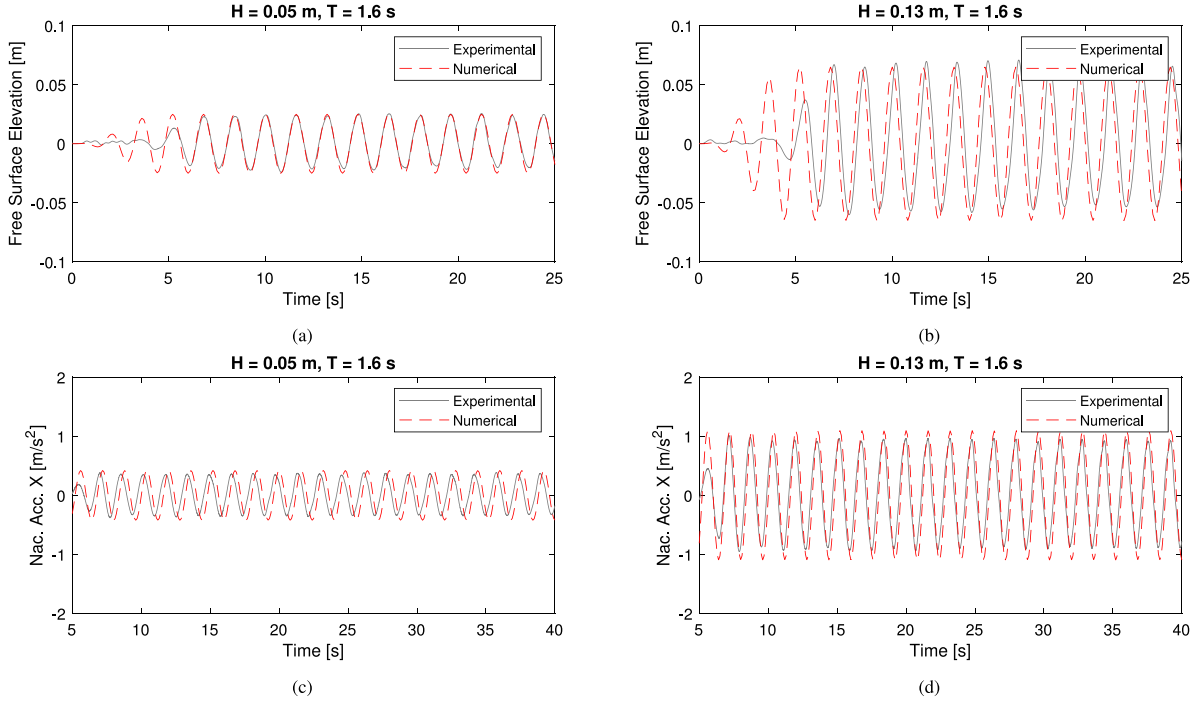

Fig. 5. Comparison between numerical and experimental results for free surface elevation (a–b) and nacelle acceleration (c–d) in time domain for Test 1 and Test 2.

speeds: a Below Rated speed of 1.45 m/s and an Above Rated speed of 1.85 m/s. The wave characteristics and wind speed are listed in Table 5. The use of regular waves enables the isolation and examination of specific parameters, thereby avoiding the complexities of non-linear phenomena that are often challenging to attribute to individual effects or parameters. This isolation enables a detailed examination of their impact on the system, which is crucial for understanding the underlying dynamics and interactions within the studied context. In this paper, regular waves are used to simplify the isolation of the effects of wind and operating conditions on the tension in the mooring lines. These tests were conducted to evaluate the tension in the mooring lines within the operating range of the wind turbine under analysis. The numerical results for surge displacement, the major contribution to mooring line solicitation, and effective mooring tension were evaluated in both the time domain and Power Spectral Density (PSD) analysis, similar to the validation phase.

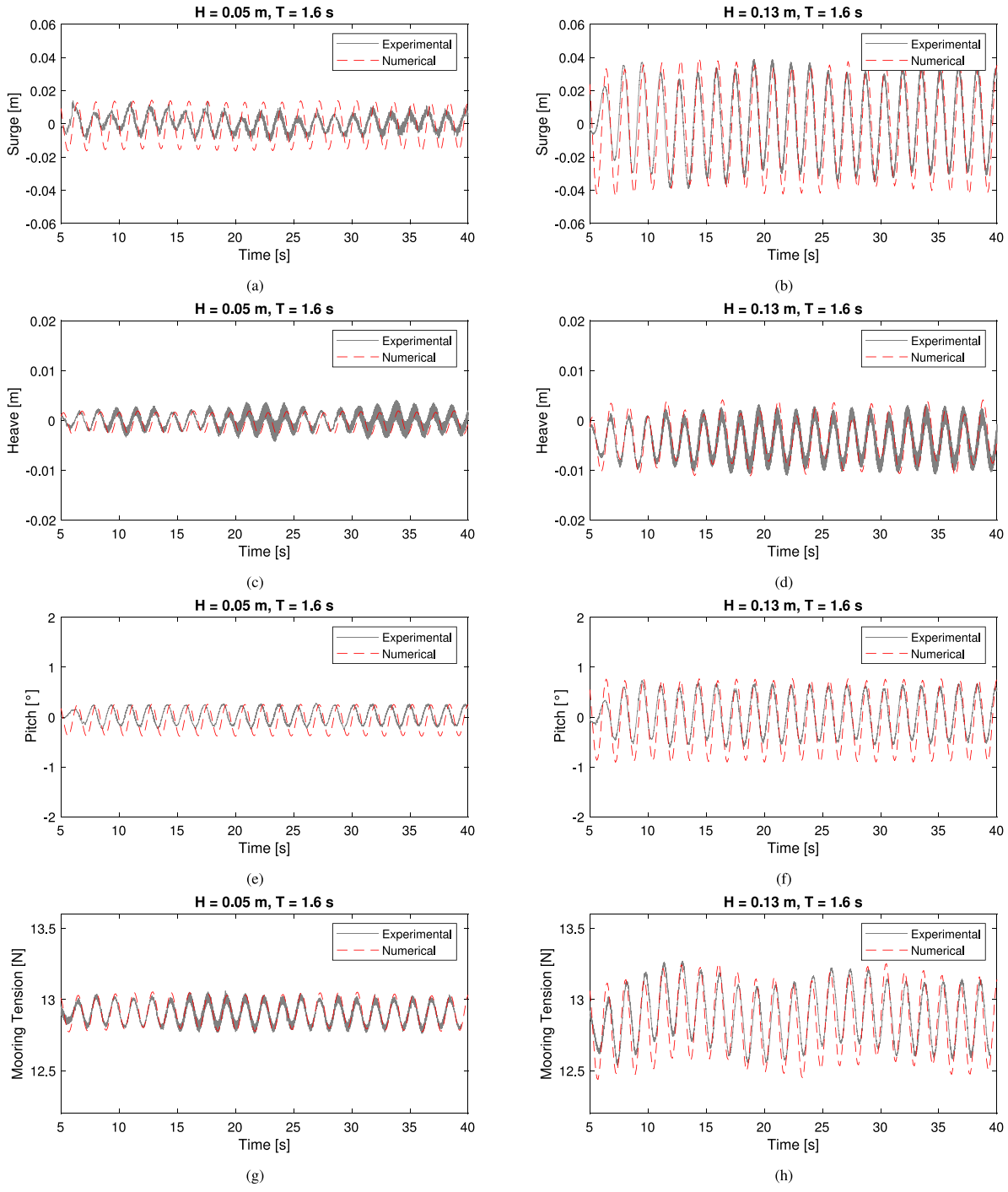

Fig. 6. Comparison between numerical and experimental results for surge (a–b), heave (c–d), pitch (e–f) and mooring tension (g–h) in time domain for Test 1 and Test 2.

Table 5
Load analysis overview.

Test number –	Wind speed [m/s]	Waves –	H_s [m]	T_s [s]	Direction [deg]
1	0	Regular	0.05	1.6	0
2	0	Regular	0.13	1.6	0
3	1.45	Regular	0.05	1.6	0
4	1.45	Regular	0.13	1.6	0
5	1.85	Regular	0.05	1.6	0
6	1.85	Regular	0.13	1.6	0

The results of the computational simulations are presented graphically in Figs. 9, 10, and 11. These figures show the comparative analyses of structure surge displacement, tension of the downwind mooring line (denoted as mooring line 1 in Fig. 2), and one of the upwind mooring lines (specifically, mooring lines 2 in Fig. 2). The choice to show the results for mooring line 2 among the two upwind mooring lines stems from their similar behavior in terms of displacement and tension. Within each image, a comparison is made between the results obtained from wave-only and operating conditions simulations. In particular, a significant observation can be made by examining the results in terms of power spectral density (PSD). Remarkably, the peak frequency of the overall response remains constant at about 0.62 Hz in both wave-only and operational conditions, aligning with the peak

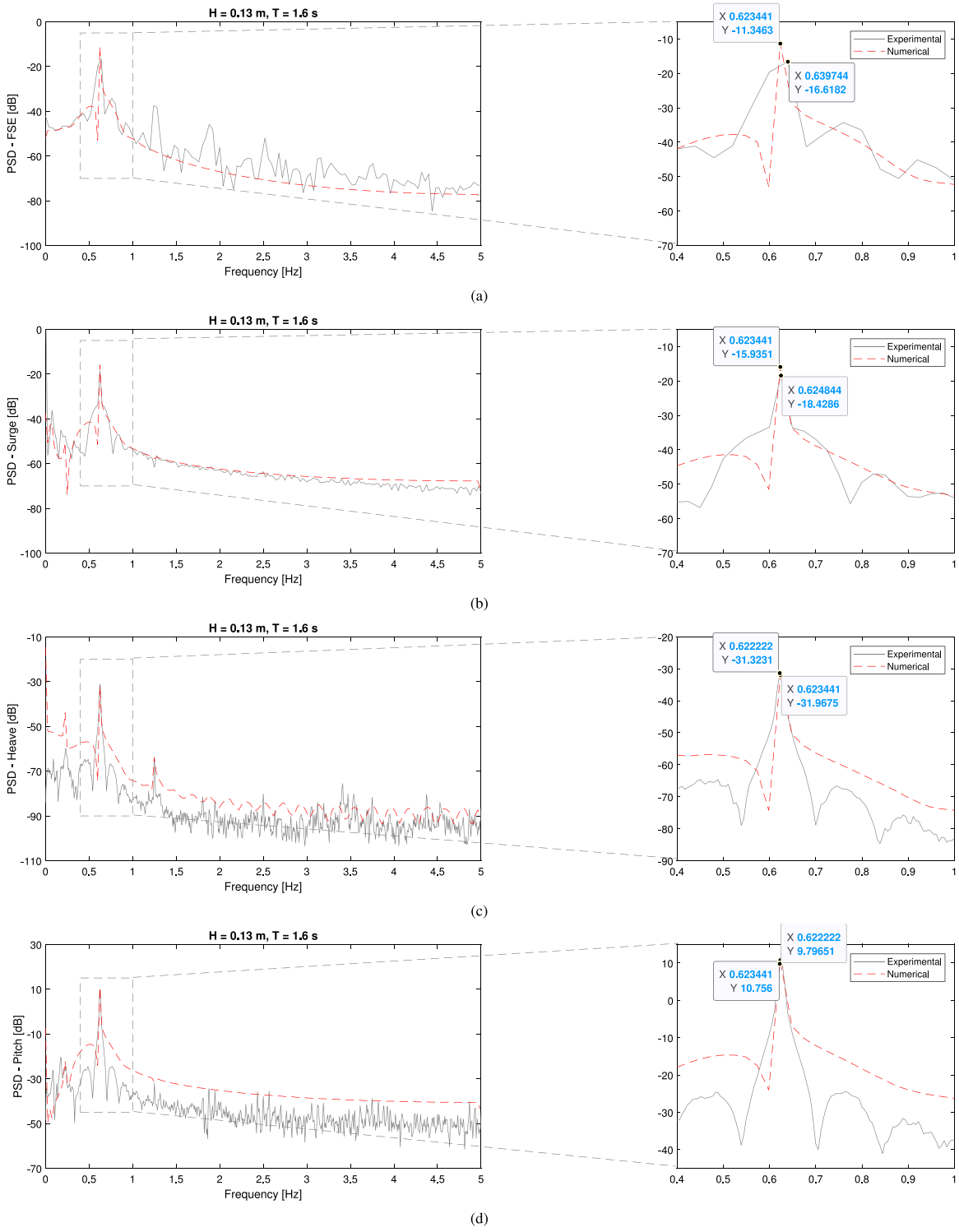

Fig. 7. Comparison between numerical and experimental PSD results of free surface elevation (a), surge (b), heave (c) and pitch (d) for Test 1.

frequency of wave action. This result emphasizes that, despite the concomitant influence of wind action and blade rotation under operating conditions, the predominant effects on the overall frequency response are mainly determined by wave action. In addition, as the height of the acting wave increases, the response of the structure manifests a higher energy content. Time domain response analysis provides insights into the variations in displacement and tension of the mooring lines during operating conditions. As the acting wave height increases, the turbine displacements undergo a corresponding increase. It is important to note that in scenarios where wave motion, wind action, and turbine operation coact, the range of displacements experienced by the buoyant structure is considerably wider than in situations involving wave motion alone. This variation intensifies with increasing wind speed and the frequency of rotor rotation. Furthermore, the displacement time series reveals two distinct oscillation periods: the first, contingent on the wave period, and the second, contingent on the wind and rotor rotation period. For instance, at a wind speed of 1.45 m/s, the rotor rotation frequency is 7.04 rad/s, while at a wind speed of 1.85 m/s, it increases

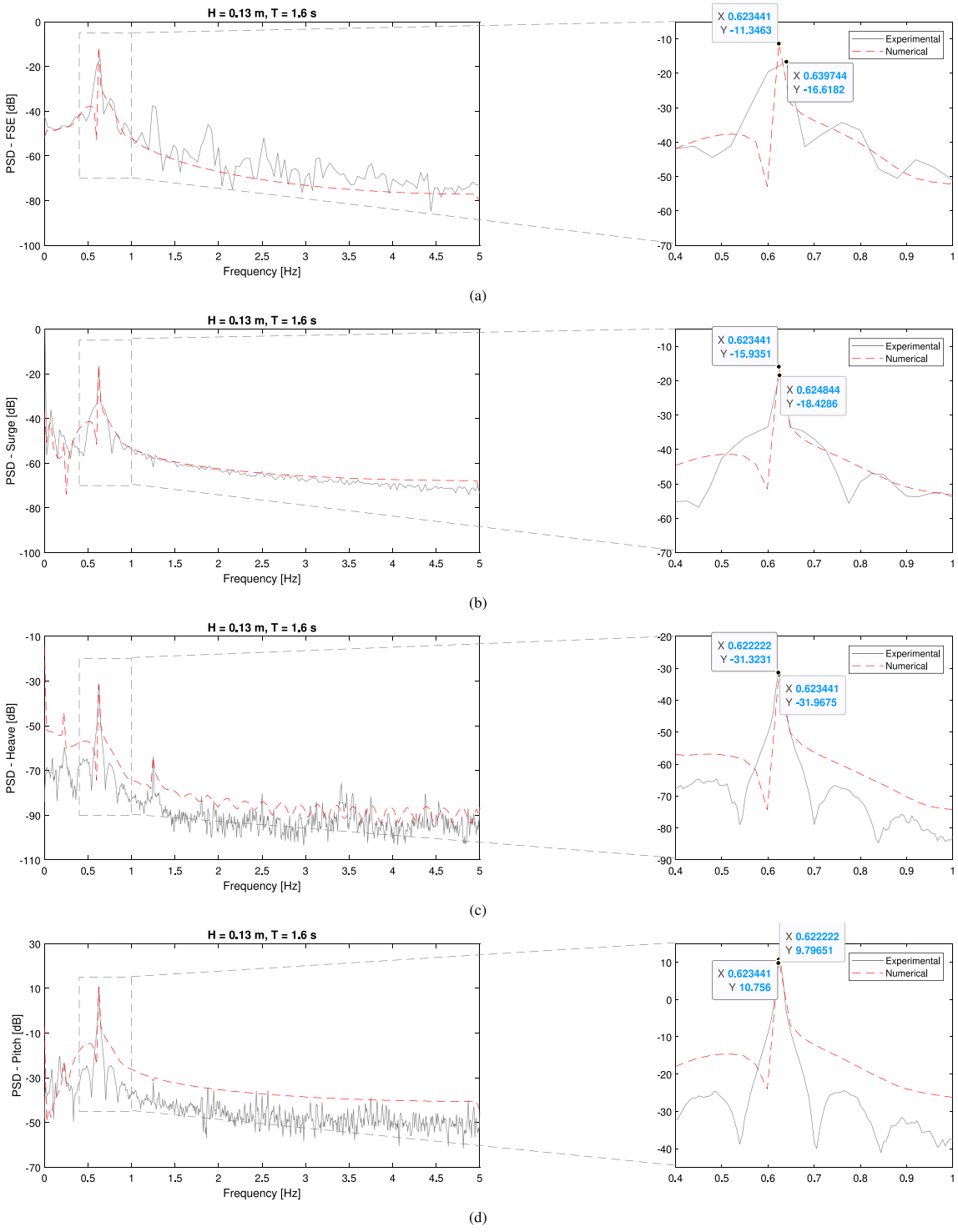

Fig. 8. Comparison between numerical and experimental PSD results of free surface elevation (a), surge (b), heave (c), pitch (d) for Test 2.

to 7.85 rad/s. This differentiation in the displacement field has repercussions on axial tensile stresses in the mooring lines. Shifting from a symmetrical response with respect to the origin in the two directions parallel to wave action to an asymmetrical response leads to variations in mooring line tensions. Consistent with displacements predominantly aligned with the wave direction, the downwind mooring line experiences detensioning (Fig. 10(a–b)), while upwind mooring lines undergo increased tension (Fig. 11(a–b)). Additionally, with increasing wave height, the disparity between average tensions in wave-only conditions versus operational conditions amplifies. A noteworthy effect for all mooring lines is the fluctuation in the service tension range during operational conditions, which surpasses the range observed in wave-only conditions. Detailed numerical values are provided in Table 6, offering a deeper understanding of this phenomenon in terms of mean, minimum and maximum tension.

3.2. Most probable maximum value statistic analysis

From the analysis of the dynamic behavior of the wind turbine in operating conditions, it is evident that in operational scenarios, the

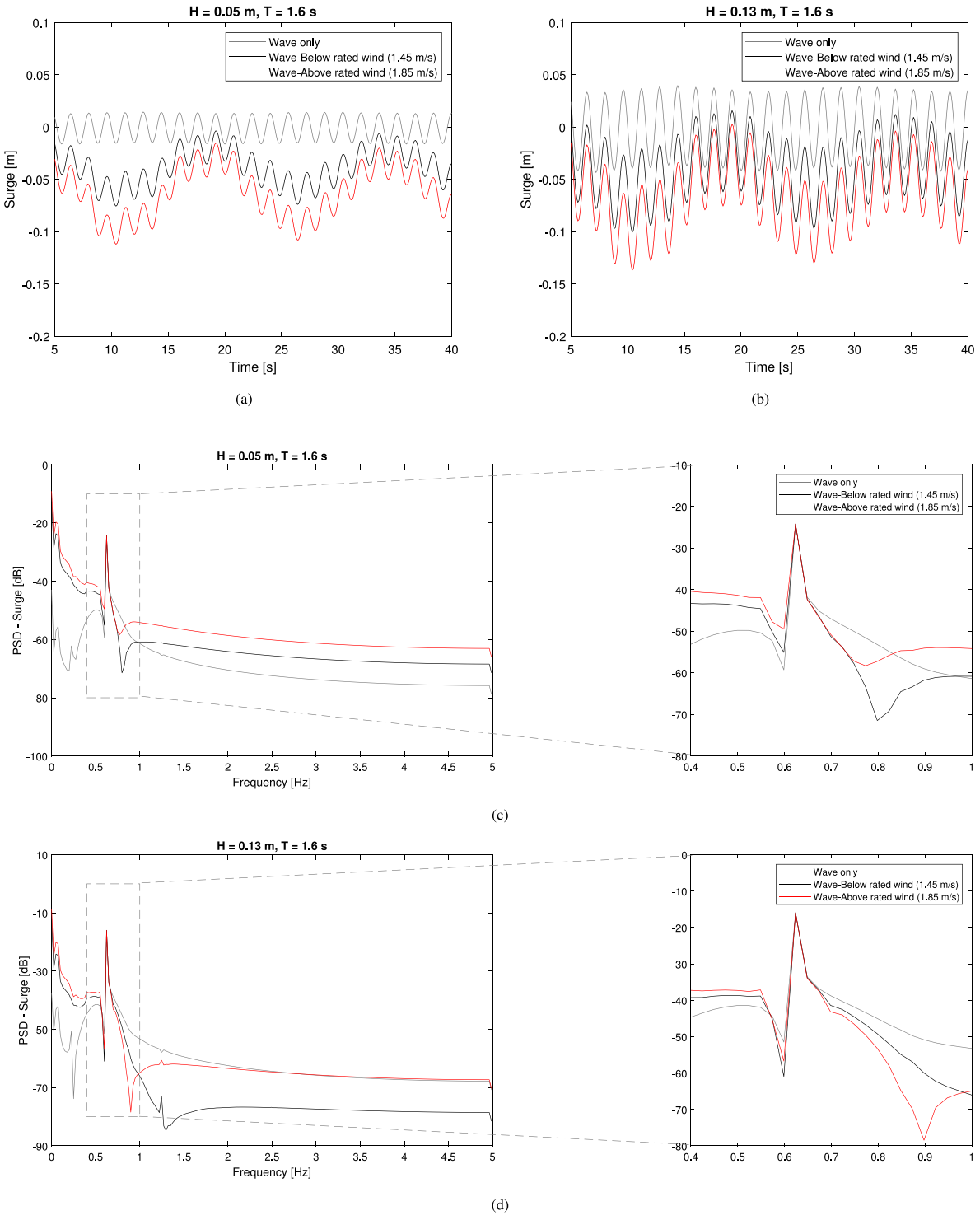

Fig. 9. Comparison between numerical results for surge displacement in no wind condition and the two operating condition, in terms of time domain and Power Spectral Density (PSD).

coexistence of wind action along with wave action profoundly affect the displacement time series of floating wind turbines. This interplay results in significant variations in the tensile stresses experienced by the mooring lines. The modified response is characterized by changes in average tension values and an expansion of the operational range of mooring line tension. Specifically, upwind mooring line endure heightened tensions under operational conditions compared to wave-only conditions, while downwind mooring lines experience reduced tensions. Nevertheless, the entire mooring system encounters a wider range of stress levels. Being able, therefore, to summarize the effects of the operating conditions on the mooring lines through the mean, maximum and minimum tension values, it is possible to treat the results statistically. Analyzing the data statistically allowed us to overcome the temporal limitations of the numerical analyses performed by evaluating the most probable long-term effects that operating conditions would induce on mooring lines. In particular, employing statistical extreme value theory facilitated the identification of the most probable maximum stress value under specified wave and wind conditions over an

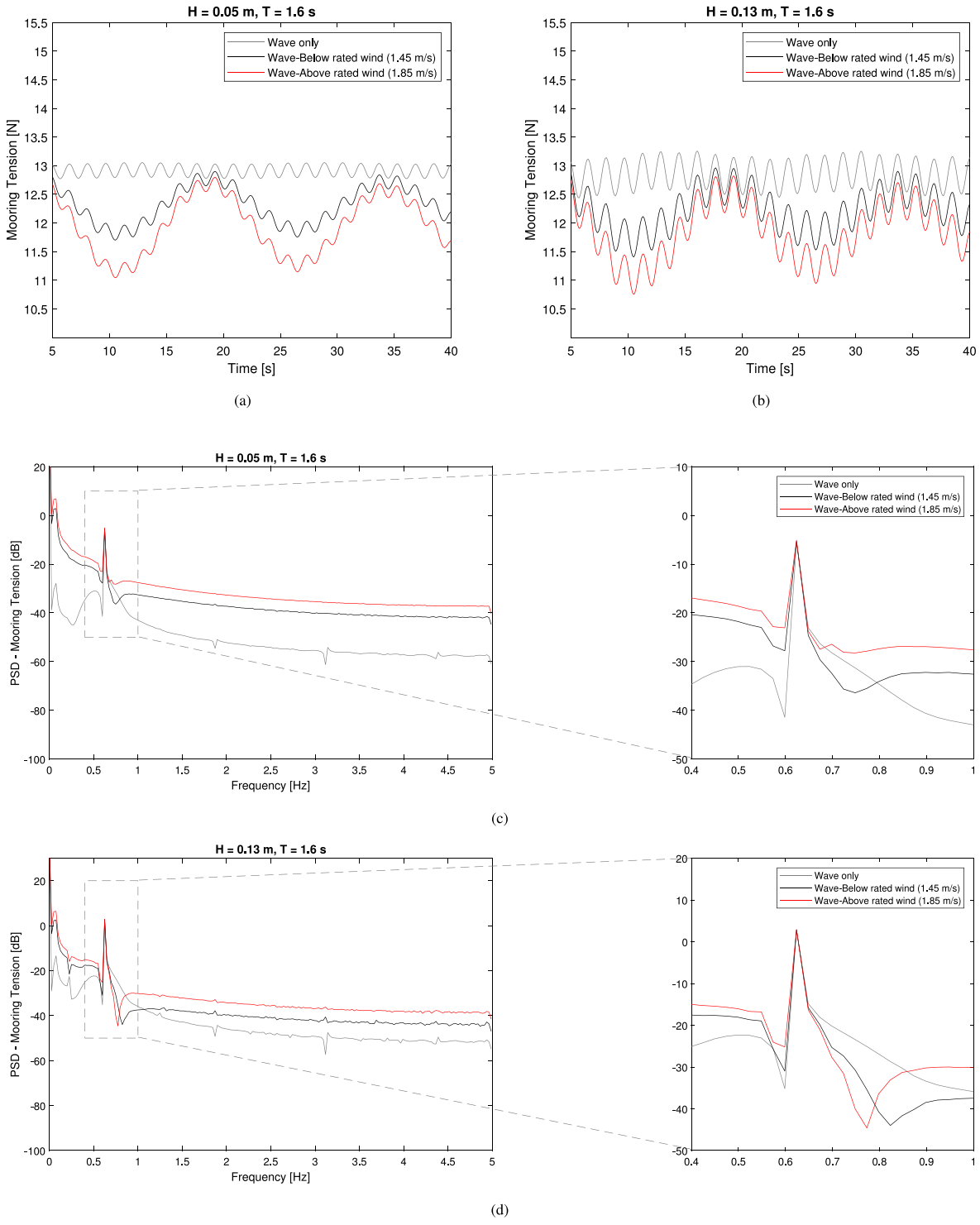

Fig. 10. Comparison between numerical results at mooring line 1 tension in no wind condition and the two operating condition, in terms of time domain and Power Spectral Density (PSD).

extended duration. This evaluation employed the Rayleigh statistical distribution method for tests conducted in OrcaFlex, considering characteristic durations of the investigated agent actions of 3, 6, 9, 12, and 24 h. Three distinct risk factors (the probability that the extreme value can be exceeded) of 1%, 2%, and 5%, corresponding to return periods of 100 years, 50 years, and 20 years, respectively, were applied to evaluate the long-term effects. The results, detailed in Tables 7 and 8 for mooring line 1, and Tables 9 and 10 for mooring line 2, were subsequently compared graphically in Figs. 12 and 13.

Each figure, delineated for a specific risk factor and wave height, presents a comparison between Most Probable Maximum (MPMs) value of tension obtained in wave-only and operational condition tests for each of the considered durations. The obtained results, presented in both tabular and graphical formats, offer compelling insights. Firstly, an observation reveals that with an increasing considered duration, the maximum tension values exhibit an ascending trend, whereas an increase in the risk factor corresponds to a decrease in these values. Notably, operating conditions induce significantly higher maximum

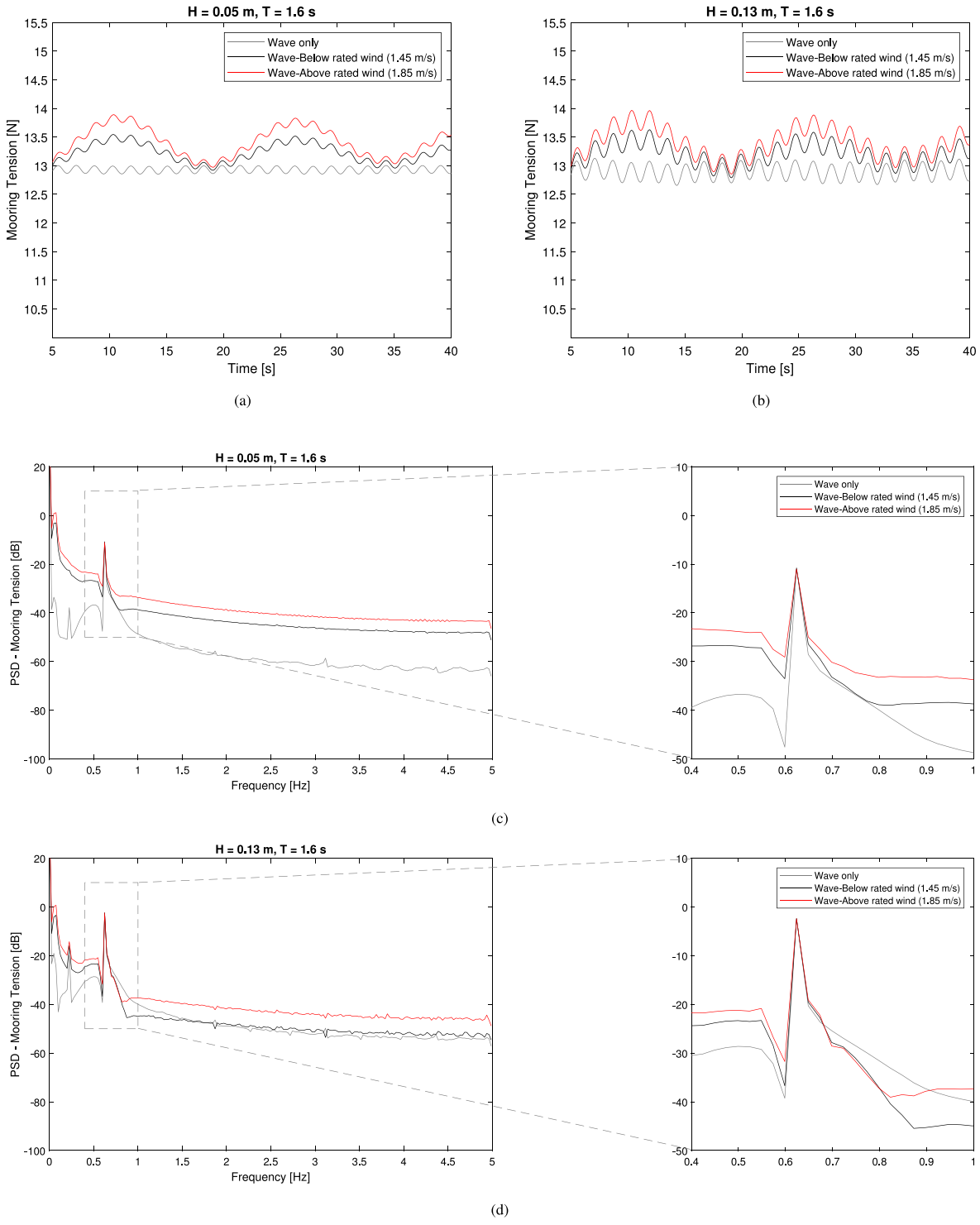

Fig. 11. Comparison between numerical results at mooring line 2 tension in no wind condition and the two operating condition, in terms of time domain and Power Spectral Density (PSD).

tension values compared to those observed in wave-only conditions. Furthermore, these tension values escalate with an increase in the acting wind and, consequently, the rotor rotation. It is also noteworthy that, under wave-only conditions, the maximum tension value experiences a substantial increase with rising wave height. However, this increase is less emphasized when considering the variation in wave height associated with a specific operating condition. This effect appears evident by comparing Figs. 12 and 13a–c–e respectively with Figs. 12 and 13b–d–f. This demonstrates a dual impact of operating conditions on mooring line stresses. On one hand, they elevate maximum tension values significantly compared to wave-only scenarios, while concurrently offering substantial damping of contributions attributed to wave motion. To reveal the underlying relationships between the variables, these discussed variation trends are extrapolated and visually

Table 6
Mean, maximum and minimum value of tension for mooring line 1 and mooring line 2 for the different tests considered.

		Mooring 1			Mooring 2		
		Mean tension [N]	Min tension [N]	Max tension [N]	Mean tension [N]	Min tension [N]	Max tension [N]
H = 0.05 m T = 1.6 s	Wave only	12.913	12.771	13.054	12.929	12.850	13.005
	Wave_Below rated wind	12.385	11.699	12.986	13.191	12.893	13.544
	Wave_Above rated wind	12.059	11.043	12.970	13.358	12.898	13.889
H = 0.13 m T = 1.6 s	Wave Only	12.853	12.436	13.255	12.899	12.654	13.129
	Wave_Below rated wind	12.299	11.406	13.110	13.174	12.788	13.628
	Wave_Above rated wind	11.965	10.752	13.094	13.344	12.814	13.964

Table 7
Extreme value statistics analysis results for mooring 1 tension with wave H = 0.05 m and T = 1.6 s.

Extreme value statistics analysis - Mooring 1 - Tension : Regular wave H = 0.05 m, T = 1.6 s								
Wave only			Wave-Below rated wind (1.45 m/s)			Wave-Above rated wind (1.85 m/s)		
Storm duration [h]	Risk factor [%]	Mooring tension [N]	Storm duration [h]	Risk factor [%]	Mooring tension [N]	Storm duration [h]	Risk factor [%]	Mooring tension [N]
3	1	13.365	3	1	14.131	3	1	14.734
6	1	13.377	6	1	14.179	6	1	14.811
9	1	13.383	9	1	14.208	9	1	14.857
12	1	13.388	12	1	14.228	12	1	14.887
24	1	13.399	24	1	14.274	24	1	14.960
3	2	13.353	3	2	14.079	3	2	14.654
6	2	13.365	6	2	14.130	6	2	14.734
9	2	13.372	9	2	14.159	9	2	14.779
12	2	13.377	12	2	14.179	12	2	14.811
24	2	13.388	24	2	14.227	24	2	14.881
3	5	13.337	3	5	14.010	3	5	14.543
6	5	13.349	6	5	14.062	6	5	14.626
9	5	13.356	9	5	14.092	9	5	14.673
12	5	13.361	12	5	14.113	12	5	14.706
24	5	13.373	24	5	14.163	24	5	14.785

Table 8
Extreme value statistics analysis results for mooring 1 tension with wave H = 0.13 m and T = 1.6 s.

Extreme value statistics analysis - Mooring 1 - Tension: Regular wave H = 0.13 m, T = 1.6 s								
Wave only			Wave-Below rated wind (1.45 m/s)			Wave-Above rated wind (1.85 m/s)		
Storm duration [h]	Risk factor [%]	Mooring tension [N]	Storm duration [h]	Risk factor [%]	Mooring tension [N]	Storm duration [h]	Risk factor [%]	Mooring tension [N]
3	1	14.045	3	1	14.353	3	1	14.798
6	1	14.076	6	1	14.407	6	1	14.876
9	1	14.093	9	1	14.438	9	1	14.921
12	1	14.106	12	1	14.460	12	1	14.952
24	1	14.315	24	1	14.511	24	1	15.027
3	2	14.014	3	2	14.298	3	2	14.717
6	2	14.045	6	2	14.353	6	2	14.797
9	2	14.063	9	2	14.385	9	2	14.843
12	2	14.076	12	2	14.407	12	2	14.876
24	2	14.105	24	2	14.459	24	2	14.952
3	5	13.971	3	5	14.221	3	5	14.604
6	5	14.003	6	5	14.278	6	5	14.688
9	5	14.022	9	5	14.311	9	5	14.736
12	5	14.035	12	5	14.334	12	5	14.770
24	5	14.065	24	5	14.388	24	5	14.849

depicted in a dimensionless format in Fig. 14. Adimensionalizing these parameters involved scaling them with respect to the maximum values obtained for each variables, so that the resulting dimensionless parameters are independent of the units of measurement. Specifically for the two mooring lines under examination, the graphical representation contrasts the variation trends of MPM tension concerning risk factor and duration for wave-only and operating condition tests across varying wave heights. Throughout all tests, irrespective of the actions involved, tension values rise with increasing duration and decline as the risk factor increases. Notably, these fluctuations are more pronounced in operating conditions. A significant observation in this context is the impact of wave height in operating conditions on mooring line tensions. In wave-only scenarios, noticeable variations in results emerge when comparing two different wave heights, but in operating condition, the tension values tend to coincide as the wind action and the consequent rotation of the rotor increase even if two waves of different heights are considered. The last significant finding in the results presented reveals an intriguing phenomenon. In numerical dynamic analyses conducted under operating conditions, where the displacement response evolves over time, the mooring lines show different tension fluctuations. Mooring line 1 (Fig. 10a–b) shows a decrease in tension values compared to the wave-only simulation, while Mooring line 2 (Fig. 11a–b) show an increase. However, MPM value statistical analysis revealed a consistent overall increase in tensions across all mooring lines under operating conditions, with mooring line 1 surprisingly showing the highest values with notable frequency. Deepening the statistical framework (Eq. (22)) and aligning it with previous observations, it becomes clear that the standard deviation σ is a key parameter that drive this phenomenon,

Table 9
Extreme value statistics analysis results for mooring 2 tension with wave H = 0.05 m and T = 1.6 s.

Extreme value statistics analysis - Mooring 2 - Tension: Regular wave H = 0.05 m, T = 1.6 s								
Wave only			Wave-Below rated wind (1.45 m/s)			Wave-Above rated wind (1.85 m/s)		
Storm duration [h]	Risk factor [%]	Mooring tension [N]	Storm duration [h]	Risk factor [%]	Mooring tension [N]	Storm duration [h]	Risk factor [%]	Mooring tension [N]
3	1	13.178	3	1	14.072	3	1	14.730
6	1	13.184	6	1	14.097	6	1	14.770
9	1	13.188	9	1	14.111	9	1	14.793
12	1	13.190	12	1	14.121	12	1	14.809
24	1	13.196	24	1	14.145	24	1	14.846
3	2	13.171	3	2	14.046	3	2	14.689
6	2	13.178	6	2	14.072	6	2	14.730
9	2	13.181	9	2	14.086	9	2	14.754
12	2	13.184	12	2	14.097	12	2	14.770
24	2	13.190	24	2	14.121	24	2	14.808
3	5	13.162	3	5	14.010	3	5	14.632
6	5	13.169	6	5	14.037	6	5	14.675
9	5	13.173	9	5	14.052	9	5	14.699
12	5	13.175	12	5	14.063	12	5	14.716
24	5	13.182	24	5	14.088	24	5	14.756

Table 10
Extreme value statistics analysis results for mooring 2 tension with wave H = 0.13 m and T = 1.6 s.

Extreme value statistics analysis - Mooring 2 - Tension: Regular wave H = 0.13 m, T = 1.6 s								
Wave only			Wave-Below rated wind (1.45 m/s)			Wave-Above rated wind (1.85 m/s)		
Storm duration [h]	Risk factor [%]	Mooring tension [N]	Storm duration [h]	Risk factor [%]	Mooring tension [N]	Storm duration [h]	Risk factor [%]	Mooring tension [N]
3	1	13.558	3	1	14.212	3	1	14.779
6	1	13.574	6	1	14.239	6	1	14.818
9	1	13.584	9	1	14.255	9	1	14.841
12	1	13.591	12	1	14.266	12	1	14.857
24	1	13.607	24	1	14.292	24	1	14.895
3	2	13.540	3	2	14.184	3	2	14.738
6	2	13.557	6	2	14.212	6	2	14.778
9	2	13.567	9	2	14.228	9	2	14.802
12	2	13.574	12	2	14.239	12	2	14.818
24	2	13.591	24	2	14.266	24	2	14.857
3	5	13.516	3	5	14.146	3	5	14.681
6	5	13.534	6	5	14.175	6	5	14.723
9	5	13.544	9	5	14.191	9	5	14.748
12	5	13.552	12	5	14.203	12	5	14.765
24	5	13.568	24	5	14.230	24	5	14.805

which in this case is related to the wide range of tensions experienced by the mooring lines (Figs. 10a–b and 11a–b). In fact, it can be seen both from the figures just mentioned and by looking at the data shown in the Table 6, mooring line 1 is the one with the greatest difference between the minimum and maximum tension values. An increase in standard deviation corresponds to an increase in MPM tension regardless of whether the outputs related to tension values were higher or lower during the numerical analyses in the operating condition than in the wave-only condition. This underscores that one of the most significant effects induced by operating conditions, particularly relevant when considering long-term implications, is the wide variability in the tensions experienced by mooring lines.

4. Conclusions

A crucial and extensively discussed research domain focuses on investigating the effects induced by the wave-wind interaction on floating structures, particularly emphasizing the dynamics during operating conditions. This field of study holds significant importance in safeguarding structures from substantial damage. Central to ensuring stability during operational phases is the critical role played by the mooring system within the structure. The aim of this paper is to offering valuable insights into the impact of operating conditions on the mooring systems of floating offshore wind turbines. This study seeks to specifically examine and understand the influence of offshore wind turbine operating conditions on the dynamics and tension characteristics of mooring lines, with a specific focus on the spar-type design. A validated numerical model implemented in OrcaFlex was employed to support the analysis of dynamic conditions involving combined wave-wind action and an operational turbine, while also assessing long-term effect.

The following are the most significant findings derived from the analyses:

- the peak frequency is primarily influenced by the wave frequency and remains unaltered by the operating conditions;
- operating conditions lead to fluctuations in the structure's displacement response, resulting in notable alterations in the tension distribution within the mooring lines;
- operating conditions induce high tension levels in mooring lines, particularly for prolonged periods, while also exerting a damping effect related to wave-induced effects;
- the predominant negative impact of operating conditions on mooring lines is manifested by the widening of the operating tension range.

The potential consequences of high mooring line tension under operating condition are multifaceted, especially when considering long-term effects. Firstly, the increased tension can lead to a higher risk of mooring line failure, which poses a significant safety hazard for offshore floating wind turbine. This can result in the loss of station-keeping ability, potentially leading to collisions, groundings, or other dangerous

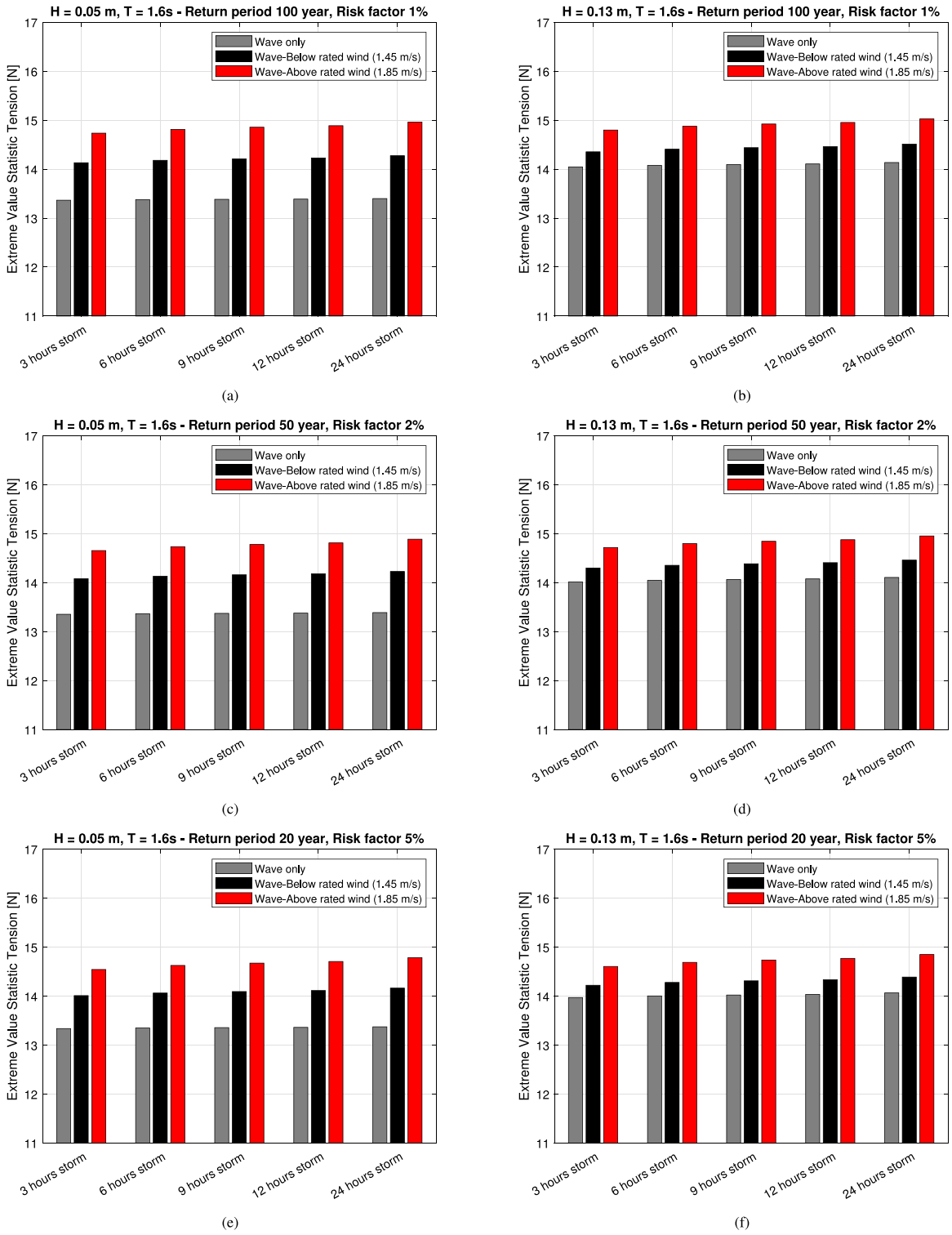

Fig. 12. Comparison between extreme value statistic for mooring 1 tension in no wind condition and the two operating condition for different risk factor corresponding to three different return period combined with different storm duration.

incidents. Moreover, the structural integrity of the mooring system itself may be compromised, impacting the overall stability and safety of the structure. Additionally, high mooring line tension can contribute to increased fatigue damage, reducing the operational lifespan of the mooring system and necessitating more frequent maintenance and replacement. Furthermore, it is crucial to carefully consider and mitigate the potential consequences of high mooring line tension under extreme conditions to ensure the safety and reliability of offshore operations.

By isolating and analyzing these impacts, our research has addressed a significant gap in the literature regarding the impact of wind and turbine operational conditions on the mooring systems of FOWTs. The results emphasize the importance of considering the combined effects of wind and wave characteristics and operating conditions when designing mooring systems, as these factors can lead to significant variations in mooring line tension, particularly considering long-term effect and extreme values, ensuring mooring system resilience and

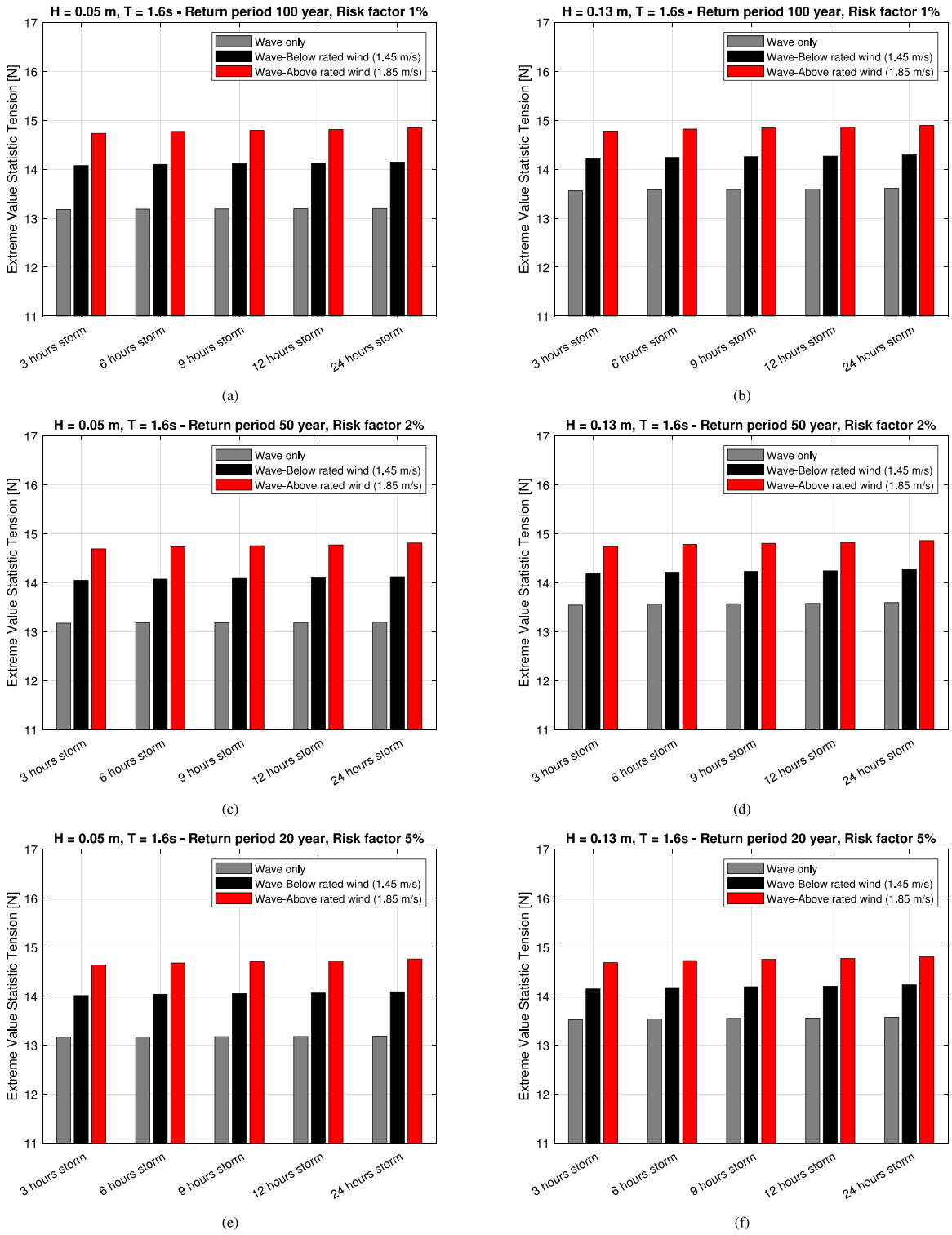

Fig. 13. Comparison between extreme value statistic for mooring 2 tension in no wind condition and the two operating condition for different risk factor corresponding to three different return period combined with different storm duration.

structural integrity under a wide range of operating conditions. The insights gained from this study not only advance the understanding of mooring dynamics but also provide a foundation for future research aimed at improving the resilience and performance of floating offshore wind technologies. In light of our findings, we recognize the importance of extending our study to encompass a broader range of conditions and scenarios. While the current research focused on regular waves, future work will aim to incorporate the effects of nonlinear waves to better simulate real-world ocean environments, such as freak wave, wave group, focused wave, etc. along with different wind scenarios that can accurately reflect the operational environment of FOWTs. Research could be extended to a full-scale numerical model exposed to the combined wave-wind interactions specific to a designated installation site. This aims to validate the observed trends or identify potential modifications under these circumstances. Another critical area for future research is the assessment of mooring line failure mechanisms.

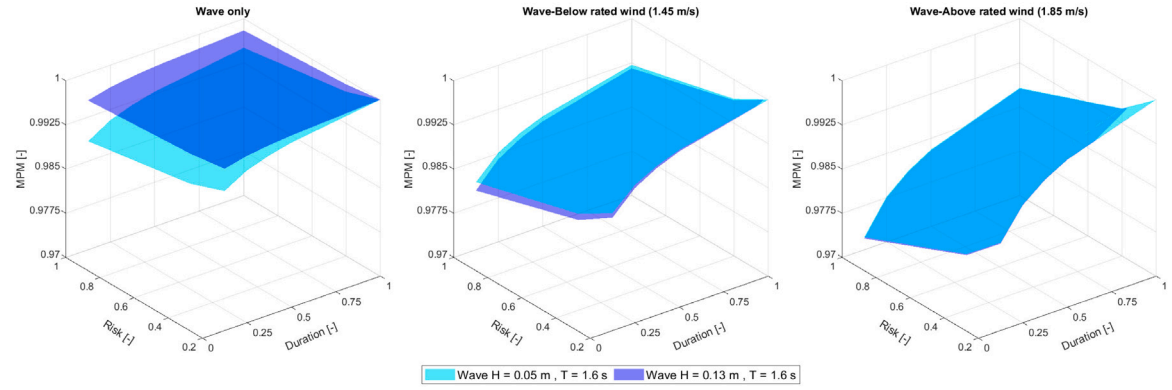

(a) Mooring line 1

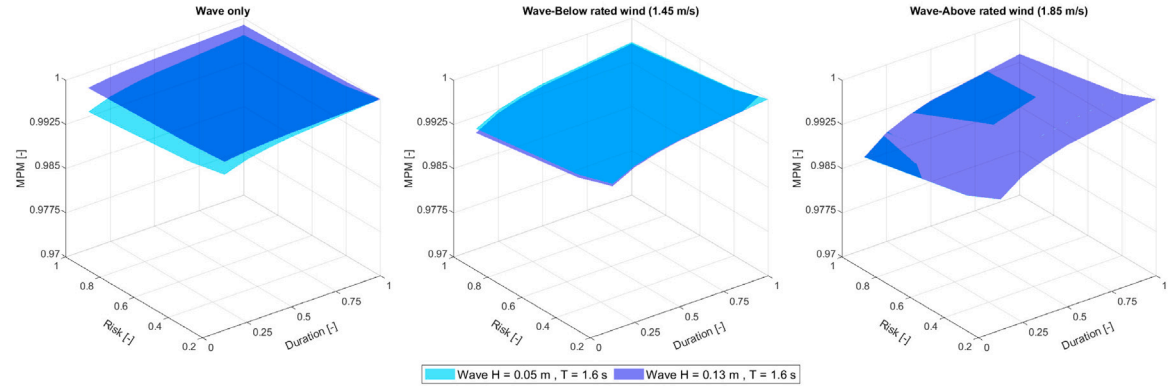

(b) Mooring line 2

Fig. 14. Dimensionless variation trends of MPM tension concerning risk factor and duration for wave-only and operating condition tests across varying wave heights.

Understanding the conditions that lead to mooring failure is essential for improving the reliability and safety of mooring systems. This will involve detailed fatigue assessments and thorough investigations under extreme loading conditions. Additionally, in-depth examinations of the specific phenomena contributing to extreme tension levels are imperative for a comprehensive understanding.

CRediT authorship contribution statement

A. Lauria: Supervision, Methodology, Investigation, Conceptualization. **P. Loprieno:** Writing – original draft, Methodology, Investigation, Formal analysis, Data curation, Conceptualization. **F. Rizzo:** Methodology, Investigation. **A. Severini:** Software, Resources. **D. Foti:** Supervision, Methodology. **E. Leone:** Writing – review & editing, Investigation, Data curation. **A. Francone:** Writing – review & editing, Investigation, Data curation. **G.R. Tomasicchio:** Supervision, Methodology, Funding acquisition.

Declaration of competing interest

The authors declare that they have no known competing financial interests or personal relationships that could have appeared to influence the work reported in this paper.

Data availability

Data will be made available on request.

Acknowledgments

The present research was funded by the European Union – Next Generation EU through the grant of the project PRIN 2022 titled "NonlinEar Phenomena in floaTing offshore wind tUrbiNEs (NEPTUNE)", Project code: 2022W7SKTL.

References

Aggarwal, N., Manikandan, R., Saha, N., 2017. Nonlinear short term extreme response of spar type floating offshore wind turbines. Ocean Eng. 130, 199–209.
Bae, Y., Kim, M., Kim, H., 2017. Performance changes of a floating offshore wind turbine with broken mooring line. Renew. Energy 101, 364–375.
Bahramiasl, S., Abbaspour, M., Karimirad, M., 2018. Experimental study on gyroscopic effect of rotating rotor and wind heading angle on floating wind turbine responses. Int. J. Environ. Sci. Technol. 15, 2531–2544.
Bak, C., Zahle, F., Bitsche, R., Kim, T., Yde, A., Henriksen, L.C., Hansen, M.H., Blasques, J.P.A.A., Gaunaa, M., Natarajan, A., 2013. The DTU 10-MW reference wind turbine. In: Danish Wind Power Research 2013.
Barrera, C., Battistella, T., Guanche, R., Losada, I.J., 2020. Mooring system fatigue analysis of a floating offshore wind turbine. Ocean Eng. 195, 106670.
Bayati, I., Belloli, M., Bernini, L., Mikkelsen, R., Zasso, A., 2016. On the aero-elastic design of the DTU 10MW wind turbine blade for the LIFES50+ wind tunnel scale model. In: Journal of Physics: Conference Series. Vol. 753, IOP Publishing, 022028.
Bayati, I., Belloli, M., Bernini, L., Zasso, A., 2017. Aerodynamic design methodology for wind tunnel tests of wind turbine rotors. J. Wind Eng. Ind. Aerodyn. 167, 217–227.
Bilgili, M., Yasar, A., Simsek, E., 2011. Offshore wind power development in Europe and its comparison with onshore counterpart. Renew. Sustain. Energy Rev. 15 (2), 905–915.
Breton, S.-P., Moe, G., 2009. Status, plans and technologies for offshore wind turbines in Europe and North America. Renew. Energy 34 (3), 646–654.
Buhl, Jr., M.L., 2005. New Empirical Relationship Between Thrust Coefficient and Induction Factor for the Turbulent Windmill State. Technical Report, National Renewable Energy Lab.(NREL), Golden, CO (United States).
Butterfield, S., Musial, W., Jonkman, J., Sclavounos, P., 2007. Engineering Challenges for Floating Offshore Wind Turbines. Technical Report, National Renewable Energy Lab.(NREL), Golden, CO (United States.
Chakrabarti, S.K., 1994. Offshore Structure Modeling, vol. 9, world scientific.
Chakrabarti, S., 2005. Handbook of Offshore Engineering (2-volume set). Elsevier.
Chen, X., Zhang, J., Johnson, P., Irani, M., 2000. Studies on the dynamics of truncated mooring line. In: ISOPE International Ocean and Polar Engineering Conference. ISOPE, pp. ISOPE–I.
Chung, J., Hulbert, G., 1993. A time integration algorithm for structural dynamics with improved numerical dissipation: the generalized-α method.

Design, A., 2005. Analysis of Station Keeping Systems for Floating Structures: API RP 2SK. API, Washington DC.
Det Norske Veritas, A., 2010. Environmental conditions and environmental loads. DNV-RP-C205.
DNV, R., 2011. H103 Modelling and Analysis of Marine Operations. Det Norske Veritas, Høvik, Norway.
Duan, F., Hu, Z., Niedzwecki, J., 2016. Model test investigation of a spar floating wind turbine. Mar. Struct. 49, 76–96.
Esteban, M.D., Diez, J.J., López, J.S., Negro, V., 2011. Why offshore wind energy? Renew. Energy 36 (2), 444–450.
Fan, T., Qiao, D., Yan, J., Chen, C., Ou, J., 2017. An improved quasi-static model for mooring-induced damping estimation using in the truncation design of mooring system. Ocean Eng. 136, 322–329.
Feist, C., Sotiropoulos, F., Guala, M., 2021. A quasi-coupled wind wave experimental framework for testing offshore wind turbine floating systems. Theor. Appl. Mech. Lett. 11 (5), 100294.
Gao, X., Liu, X., Xue, X., Chen, N.-Z., 2021. Fracture mechanics-based mooring system fatigue analysis for a spar-based floating offshore wind turbine. Ocean Eng. 223, 108618.
Goupee, A.J., Koo, B.J., Kimball, R.W., Lambrakos, K.F., Dagher, H.J., 2014. Experimental comparison of three floating wind turbine concepts. J. Offshore Mech. Arct. Eng. 136 (2), 020906.
Hsu, W.-t., Thiagarajan, K.P., Manuel, L., 2017. Extreme mooring tensions due to snap loads on a floating offshore wind turbine system. Mar. Struct. 55, 182–199.
ITTC, 2021a. Recommended procedures and guidelines - 7.5-02-07-03.1 floating offshore platform experiments. p. 12.
ITTC, 2021b. Recommended procedures and guidelines - 7.5-02-07-08.8 model tests for offshore wind turbines. p. 19.
Koo, B.J., Goupee, A.J., Kimball, R.W., Lambrakos, K.F., 2014. Model tests for a floating wind turbine on three different floaters. J. Offshore Mech. Arct. Eng. 136 (2), 020907.
Lauria, A., Loprieno, P., Francone, A., Leone, E., Tomasicchio, G., 2024. Recent advances in understanding the dynamic characterization of floating offshore wind turbines. Ocean Eng. 307, 118189.
Lee, C.F., Cheng, Z., Ong, M.C., Wang, K., 2023. Extreme response analysis of a floating vertical axis wind turbine based on modified environmental contour method. Ocean Eng. 270, 113459.
Li, X., Zhang, W., 2020. Long-term fatigue damage assessment for a floating offshore wind turbine under realistic environmental conditions. Renew. Energy 159, 570–584.
Ning, A., Hayman, G., Damiani, R., Jonkman, J.M., 2015. Development and validation of a new blade element momentum skewed-wake model within AeroDyn. In: 33rd Wind Energy Symposium. p. 0215.
Ochi, M.K., 1973. On prediction of extreme values. J. Ship Res. 17 (01), 29–37.
Ochi, M., 1998. Ocean waves: the stochastic approach. Oceanogr. Lit. Rev. 6 (45), 904.
Oguz, E., Clelland, D., Day, A.H., Incecik, A., López, J.A., Sánchez, G., Almeria, G.G., 2018. Experimental and numerical analysis of a TLP floating offshore wind turbine. Ocean Eng. 147, 591–605.
Orcina Ltd, 2024. Orcaflex documentation. URL https://www.orcina.com/webhelp/OrcaFlex/Default.htm.
Øye, S., 1986. Unsteady wake effects caused by pitch–angle changes. In: IEA R&D WECS Joint Action on Aerodynamics of Wind Turbines, 1st Symposium. pp. 58–79.
Øye, S., 1990. A simple vortex model of a turbine rotor.
Pitt, D.M., Peters, D.A., 1980. Theoretical prediction of dynamic-inflow derivatives.
Riefolo, L., del Jesus, F., Guanche García, R., Tomasicchio, G.R., Pantusa, D., 2018. Wind/wave misalignment effects on mooring line tensions for a spar buoy wind turbine. In: International Conference on Offshore Mechanics and Arctic Engineering. Vol. 51203, American Society of Mechanical Engineers, V001T01A063.
RP, A., et al., 2014. Derivation of metocean design and operating conditions. In: API.
Russo, S., Contestabile, P., Bardazzi, A., Leone, E., Iglesias, G., Tomasicchio, G.R., Vicinanza, D., 2021. Dynamic loads and response of a spar buoy wind turbine with pitch-controlled rotating blades: An experimental study. Energies 14 (12), 3598.
Saenz-Aguirre, A., Ulazia, A., Ibarra-Berastegi, G., Saenz, J., 2022. Floating wind turbine energy and fatigue loads estimation according to climate period scaled wind and waves. Energy Convers. Manage. 271, 116303.
Soares-Ramos, E.P., de Oliveira-Assis, L., Sarrias-Mena, R., Fernández-Ramírez, L.M., 2020. Current status and future trends of offshore wind power in Europe. Energy 202, 117787.
Stansberg, C., Karlsen, S., Ward, E., Wichers, J., Irani, M., 2004. Model testing for ultradeep waters. In: Offshore Technology Conference. OTC, pp. OTC–16587.
Stansberg, C.T., Ormberg, H., Oritsland, O., 2002. Challenges in deep water experiments: hybrid approach. J. Offshore Mech. Arct. Eng. 124 (2), 90–96.
Tomasicchio, G.R., Avossa, A.M., Riefolo, L., Ricciardelli, F., Musci, E., D'Alessandro, F., Vicinanza, D., 2017. Dynamic modelling of a spar buoy wind turbine. In: International Conference on Offshore Mechanics and Arctic Engineering. 57786, American Society of Mechanical Engineers, V010T09A083.
Tomasicchio, G.R., D'Alessandro, F., Avossa, A.M., Riefolo, L., Musci, E., Ricciardelli, F., Vicinanza, D., 2018. Experimental modelling of the dynamic behaviour of a spar buoy wind turbine. Renew. Energy 127, 412–432.
Tomasicchio, G.R., Vicinanza, D., Belloli, M., Lugni, C., Latham, J.-P., Rodriguez, J.G.I., Jensen, B., Vire, A., Monbaliu, J., Taruffi, F., et al., 2020. Physical model tests on spar buoy for offshore floating wind energy converion. Ital. J. Eng. Geol. Environ. 129–143.
Veritas, D.N., 2010. DNV-OS-F201 dynamic risers.
Wen, B., Jiang, Z., Li, Z., Peng, Z., Dong, X., Tian, X., 2022. On the aerodynamic loading effect of a model Spar-type floating wind turbine: An experimental study. Renew. Energy 184, 306–319.
Willis, D., Niezrecki, C., Kuchma, D., Hines, E., Arwade, S., Barthelmie, R., DiPaola, M., Drane, P., Hansen, C., Inalpolat, M., et al., 2018. Wind energy research: State-of-the-art and future research directions. Renew. Energy 125, 133–154.
Xu, H., Rui, S., Shen, K., Guo, Z., 2023. Investigations on the mooring safety considering the coupling effect of the mooring line snap tension and anchor out-of-plane loading. Appl. Ocean Res. 141, 103753.
Yang, Y., Bashir, M., Wang, J., Michailides, C., Loughney, S., Armin, M., Hernández, S., Urbano, J., Li, C., 2020. Wind-wave coupling effects on the fatigue damage of tendons for a 10 MW multi-body floating wind turbine. Ocean Eng. 217, 107909.
Zhang, C., Wang, S., Xie, S., He, J., Gao, J., Tian, C., 2022. Effects of mooring line failure on the dynamic responses of a semisubmersible floating offshore wind turbine including gearbox dynamics analysis. Ocean Eng. 245, 110478.